# Plasma-Enhanced Atomic Layer Deposition of HfO2 with Substrate Biasing: Thin Films for High-Reflective Mirrors

ACS APPLIED MATERIALS & INTERFACES

www.acsami.org

Research Article

# Plasma-Enhanced Atomic Layer Deposition of $HfO_2$ with Substrate Biasing: Thin Films for High-Reflective Mirrors

Vivek Beladiya, Tahsin Faraz, Paul Schmitt, Anne-Sophie Munser, Sven Schröder, Sebastian Riese, Christian Mühlig, Daniel Schachtler, Fabian Steger, Roelene Botha, Felix Otto, Torsten Fritz, Christian van Helvoirt, Wilhelmus M. M. Kessels, Hassan Gargouri, and Adriana Szeghalmi*

Cite This: *ACS Appl. Mater. Interfaces* 2022, 14, 14677−14692

Read Online

ACCESS | Metrics & More | Article Recommendations | Supporting Information

**ABSTRACT:** Tuning ion energies in plasma-enhanced atomic layer deposition (PEALD) processes enables fine control over the material properties of functional coatings. The growth, structural, mechanical, and optical properties of $HfO_2$ thin films are presented in detail toward photonic applications. The influence of the film thickness and bias value on the properties of $HfO_2$ thin films deposited at 100 °C using tetrakis(dimethylamino)hafnium (TDMAH) and oxygen plasma using substrate biasing is systematically analyzed. The $HfO_2$ films deposited without a substrate bias show an amorphous microstructure with a low density, low refractive index, high incorporation of residual hydroxyl (OH) content, and high residual tensile stress. The material properties of $HfO_2$ films significantly improved at a low bias voltage due to the interaction with oxygen ions accelerated to the film. Such $HfO_2$ films have a higher density, higher refractive index, and lower residual OH incorporation than films without bias. The mechanical stress becomes compressive depending on the bias values. Further increasing the ion energies by applying a larger substrate bias results in a decrease of the film density, refractive index, and a higher residual OH incorporation as well as crystalline inclusions. The comparable material properties of the $HfO_2$ films have been reported using tris(dimethylamino)cyclopentadienyl hafnium (TDMACpH) in a different apparatus, indicating that this approach can be transferred to various systems and is highly versatile. Finally, the substrate biasing technique has been introduced to deposit stress-compensated, crack- and delamination-free high-reflective (HR) mirrors at 355 and 532 nm wavelengths using $HfO_2$ and $SiO_2$ as high and low refractive index materials, respectively. Such mirrors could not be obtained without the substrate biasing during the deposition because of the high tensile stress of $HfO_2$, leading to cracks in thick multilayer systems. An HR mirror for 532 nm wavelength shows a high reflectance of 99.93%, a residual transmittance of ∼530 ppm, and a low absorption of ∼11 ppm, as well as low scattering losses of ∼4 ppm, high laser-induced damage threshold, low mechanical stress, and high environmental stability.

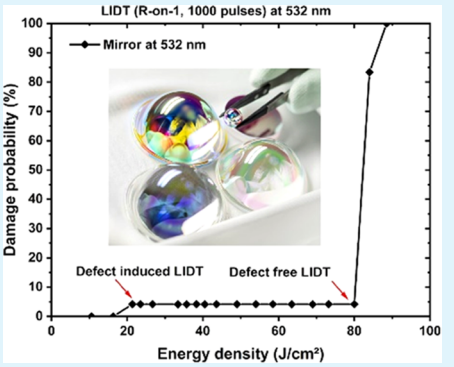


**KEYWORDS:** *plasma-enhanced ALD, substrate biasing, tailoring material properties, $HfO_2$ thin films, high-reflective mirrors, laser-induced damage threshold*



## INTRODUCTION

Hafnium dioxide ($HfO_2$) is a widely studied dielectric material due to its application in integrated circuits and optics for its high dielectric constant, high refractive index, and low optical losses in the UV spectral range down to 266 nm wavelength.[1−4] Hafnia thin films are typically used as a high refractive index material in interference coatings, especially for high-power laser applications.[5,6] $HfO_2$ thin films for optics are deposited mostly by physical vapor deposition (PVD)[4,7−10] and chemical vapor deposition (CVD)[4,8,11] techniques. Atomic layer deposition (ALD) has gained importance due to the ability to coat wide-area surfaces with excellent uniformity and grow conformal coatings on high aspect ratio nanostructured substrates.[12−19] This technology is a subclass of the CVD technique where gas-phase precursors are sequentially introduced into the deposition chamber. The layer-by-layer growth in a self-limiting manner enables ALD to deposit thin films with a precise thickness control.[20] ALD films using thermally activated reactions of reactants with surface functional groups constitute thermal ALD processes (TALD), whereas in plasma-enhanced atomic layer deposition (PEALD), the high reactivity of plasma species enables low-temperature deposition.[20−23]

$HfO_2$ thin films have been widely studied by ALD techniques, both TALD and PEALD. The material properties like density, the refractive index, impurities, defects,

Received: November 11, 2021
Accepted: February 18, 2022
Published: March 21, 2022

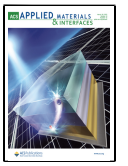




https://doi.org/10.1021/acsami.1c21889
*ACS Appl. Mater. Interfaces* 2022, 14, 14677−14692

stoichiometry, mechanical stress, and crystallinity can be optimized by varying deposition parameters like substrate temperature,[24−27] precursor dosing time,[14,27] plasma parameters,[23,27,28] and postdeposition annealing.[27,29,30] However, the range of material properties is limited, or the deposition conditions become extreme and therefore not feasible for some applications.

Recently, the substrate biasing technique has shown immense potential in PEALD thin-film development, where ion energies can be tuned by varying the bias voltage at the substrate stage to modify the material properties mentioned above.[13,31−44] Surface reactions involving enhanced reactivity and adatom diffusion are favored for ions of medium energies in the range of 30−150 eV. Ions with energies larger than 150 eV may lead to subsurface implantation, sputtering, or roughening of the PEALD thin films.[45,46] Optimum deposition conditions must be carefully evaluated to obtain thin films with appropriate properties for complex optical coatings, such as mirrors, narrow bandpass filters, beamsplitters, etc.

Metallic mirrors are widely applied in optical applications. The development and growth of metallic thin films have extensively been studied. The nucleation and the percolation of various noble metals to enhance their reflectivity have been discussed.[47−52] However, dielectric mirrors are preferred for high-power laser applications due to their higher reflectivity (>99.9%), high thermal stability, and high laser damage resistance. Despite the recent advancement in multilayer optical coatings and their application in high-power laser systems, the laser-induced damage of functional coatings is still a challenge. The laser damage of optical coatings in the nanosecond (ns) regime is attributed to thermal effects, where thermal energy is coupled into the optical coatings at the absorbing sites, embedded nodular defects, or contaminations. This leads to melting at the defect sites and to mechanical failure.[53] Also, absorption losses in these coatings can increase with nonstoichiometric defects such as oxygen vacancies or electronic defects.[53,54] Hence, high-power laser applications require coatings with low absorption and minimal nodular defects. Conventionally, high-reflective (HR) coatings are mainly prepared using PVD techniques.[54−59] Several dielectric material combinations have been used for HR coatings such as $TiO_2/SiO_2$,[60,61] $ZrO_2/SiO_2$,[60,62,63] $Nb_2O_5/SiO_2$,[60] $Al_2O_3/SiO_2$,[64,65] $Ta_2O_3/SiO_2$,[60,66,67] $Ta_2O_3/Al_2O_3$,[58] $HfO_2/SiO_2$,[54,59,68,69] and $HfO_2/Al_2O_3$.[58] The 2020 SPIE laser damage symposium evaluated the laser-induced damage threshold (LIDT) of mirrors (deposited with five different PVD methods) at 532 nm wavelength with nanosecond pulses. A mirror consisting of $HfO_2/SiO_2$ multilayers deposited by e-beam evaporation has shown the highest laser-induced damage threshold (LIDT) of 28 J/cm$^2$ (raster scan method, fluence uncertainty ∼3%, 6 ns, 100 Hz, beam diameter $(1/e^2)$ = 400 ± 4 $\mu$m) compared to mirrors deposited using other materials and coating technologies.[58] Also, $HfO_2$ and $SiO_2$ were the material of choice as the high and low refractive index layers, respectively, due to low absorption in a broad wavelength range from UV to mid-infrared.

Along with the requirements of a high LIDT, functional coatings should also show excellent mechanical stability. As the number of layers increases in a multilayer system, the increase in residual stress may lead to mechanical failures like cracking, buckling, delamination, and surface deformation.[70,71] There have been several approaches to deposit multilayers to compensate for mechanical stress. Oliver et al. incorporated alumina layers in the $HfO_2/SiO_2$ multilayer coatings to correct tensile thin-film stress.[72] Mirkarimi et al. used the athermal buffer-layer technique to deposit near-zero stress (net stress <30 MPa) for extreme ultraviolet (EUV) mirrors of Mo/Be (68.7% at 11.4 nm) and Mo/Si (66.5% at 13.3 nm) multilayers with magnetron sputtering.[73] A Mo/Be multilayer (having tensile stress) deposited on an amorphous Si athermal buffer layer (exhibiting compressive stress) and a Mo/Si multilayer (compressive stress) deposited on a Mo/Be (tensile stress) multilayer reduced the stress by >90%; meanwhile, the absolute reflectance was reduced only by <1%. de Denus-Baillargeon et al. presented two different strategies to control mechanical stress, namely, designing two complementary coatings on either side of the substrate and incorporating the mechanical properties of individual layers in the design of the optical coatings.[74] The strategies were tested by depositing a Fabry−Perot etalon used in astronomy using $SiO_2$ (compressive stress) and $TiO_2$ (tensile stress) films. The most efficient stress compensation was observed for coatings on both sides of the substrate, where the overall stress of the assembly of antireflection (AR) and reflective coating showed stress values as low as 7 MPa compared to the intrinsic stresses of −190 and +170 MPa for $SiO_2$ and $TiO_2$, respectively. The second stress-compensation method, where the mechanical stress of the single layers was incorporated into the design of the optical coating of a single side antireflection (AR), showed a 49% reduction of the total stress compared to the AR coating without incorporation of stress into the design. The strategy of depositing interference coatings on both sides of the substrate to compensate stress has also been demonstrated by Begou et al.[75,76] and Trubetskov et al.[77] Liu et al. fabricated stress-compensated AR coatings using contrary stress of $Al_2O_3$ deposited using ALD (having tensile stress) and $SiO_2$ deposited using ion beam sputtering (IBS) (having compressive stress).[78] The stress of −38 MPa ($d$ = 628 nm) was obtained for the AR coating compared to the single-layer ALD $Al_2O_3$ (302 and 343 MPa, for $d$ = 148 and 178 nm, respectively) and IBS $SiO_2$ (−450 and −315 MPa, for $d$ = 182 and 135 nm, respectively). However, complex multilayer coatings such as mirrors are difficult to coat with this strategy since the deposition has been performed in two different tools. It would be highly beneficial to control the mechanical stress in the ALD process by the process parameters.

In this work, we systematically investigate the properties of PEALD $HfO_2$ grown with substrate biasing. The stoichiometry, C and N impurities, OH contamination, roughness, mechanical stress, and optical properties of $HfO_2$ layers with different film thicknesses in the range of 30−120 nm are studied in detail. For the dielectric mirror at 355 nm wavelength, the quarter-wave thickness of $HfO_2$ is ∼60 nm, but for the mirror at 532 nm wavelength, a much thicker film of ∼90 nm is required. Therefore, in this article, the film properties were investigated as a function of film thickness. Optimized processes are applied to develop stress-compensated highly reflective coatings using PEALD. In the first part, we report on the comparative study of the substrate biasing effect on the material properties of $HfO_2$ grown in two different deposition ALD systems—the FlexAL (Oxford Instruments, Bristol, U.K.) and the SILAYO (Sentech Instruments GmbH, Berlin, Germany). In the second part, we present the effect of substrate biasing in depositing a dielectric interference mirror at 532 nm for high-power laser systems. Multilayers have been prepared using substrate biasing in PEALD, and the mechanical properties have been


https://doi.org/10.1021/acsami.1c21889
ACS Appl. Mater. Interfaces 2022, 14, 14677−14692

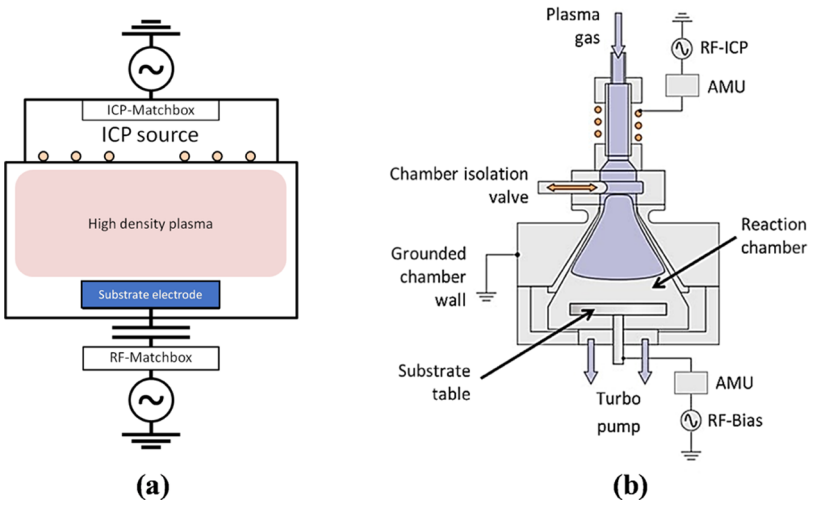


**Figure 1.** Schematic of the atomic layer deposition system: (a) the SILAYO ICP330 from Sentech instruments and (b) the FlexAL system from Oxford Instruments. RF, radio frequency; ICP, inductively coupled plasma; and AMU, automatic matching unit.

proved much better than without bias. The mirrors have been extensively investigated for LIDT and optical properties, including absorption and scattering. Finally, the environmental stability of the mirrors has been evaluated to demonstrate the high performance and stability of the ALD optics.

## EXPERIMENTAL METHODS

**SILAYO Reactor.** $HfO_2$ thin films were deposited in the SILAYO system equipped with an inductively coupled plasma (ICP) source (Sentech Instruments GmbH, Berlin, Germany), shown schematically in Figure 1a. Due to the planar design of the ICP source, a very good plasma homogeneity is possible, and optical coatings with a high uniformity over 200 mm diameter surface can be realized.[27] Additionally, a substrate biasing up to −250 V (at 2.9 Pa operating pressure) can be applied during the thin-film deposition. A dry vacuum pump is used to evacuate the chamber down to 0.02 Pa base pressure. The system is also equipped with a turbo-molecular pump to evacuate the chamber to a high vacuum whenever required. The substrate can be introduced into the deposition chamber via a load lock. Substrates of 330 mm diameter and 120 mm height can be coated using this system.

This prototype PEALD system uses a planar triple spiral antenna (PTSA) as an inductively coupled plasma source (PTSA-ICP, 500 W, 13.56 MHz radio-frequency (RF) plasma generator), and a substrate stage that can be biased by an RF generator (500 W, 13.56 MHz RF plasma generator). The PTSA-ICP plasma coil is separated from the chamber by a quartz plate (⌀ 455 mm). A voltage-peak-to-peak sensor ($V_{pp}$ box), which is installed between the RF-driven substrate electrode and its matchbox, provides information about the resulting dc bias voltage ($V_{dc}$). The system adjusts the power of the RF generator to maintain a constant $V_{dc}$ value. The value of $V_{pp}$ has not been verified yet by retarded field energy analyzer (RFEA) measurements whether this value exactly corresponds with the bias voltage, the voltage of the plasma sheath, and hence with the ion energy. Nonetheless, the properties of the $HfO_2$ films correlate very well with $V_{dc}$, even if absolute bias values are not yet determined.

In the case of low-pressure reactors, when there are no collisions in the plasma sheath, multiplying $V_{dc}$ with the ion charge gives the ion energy of the ions in eV. Using nonconductive substrates (e.g., quartz, ceramics), it is not possible to derive a conclusive value for $V_{dc}$ at the substrate. In such cases, the bias voltage $V_{dc}$ provided by the $V_{pp}$ box is not applicable to assess the energy of the ions impacting the substrate surface. Still, a related mean electric field is present, and ions are accelerated toward the substrate surface through the plasma sheath above the RF-driven substrate electrode. To determine the exact ion energies, dedicated retarded field energy analyzer (RFEA) impedance measurements are necessary, which are currently in preparation. Technically, the voltage-peak-to-peak sensor, which is installed within the PEALD system, provides a means to control the impact of ions in such applications. The measurement of the $V_{pp}$ box is independent of the substrate used and can thus facilitate process understanding, optimization, reproducibility, and process transfer.

Comparative $HfO_2$ thin films have been deposited in a FlexAL system (Oxford Instruments, Bristol, U.K.). Details of this equipment have already been published,[13] and the schematic diagram is included in Figure 1b. The similarities in the $HfO_2$ film properties made with two reactors are discussed here to assess the capability of the biasing technique.

**Single $HfO_2$ Layer.** The $HfO_2$ thin films within Silayo equipment were deposited at 100 °C using a tris(dimethylamino)hafnium (TDMAH) precursor and oxygen plasma on double side polished (DSP) c-Si(100) wafers of 76 mm diameter and ∼400 μm thickness, 25 mm diameter fused silica glass substrates of 1 mm thickness, eight small single side polished (SSP) c-Si(100) pieces (approximately 20 × 20 $mm^2$), and a 25 × 25 $mm^2$ DSP c-Si(100) piece. Four of the eight small SSP pieces were placed on the substrate plate at a distance of 100 mm diameter and four in a 200 mm diameter in a concentric pattern around the center. The TDMAH precursor container was heated at 50 °C, the ALD valves at 60 °C, the precursor delivery line at 90 °C, and the substrate table at 100 °C. Argon was used as a carrier gas with a flow rate of 160 sccm. The $O_2$ flow was 200 sccm, and the ICP power of 100 W was used for the plasma. The carrier and oxygen gases were delivered continuously to the reactor during the entire deposition. Additionally, an argon flow of 50 sccm was delivered under the substrate plate to prevent its coating. The precursor pulse, precursor purge, plasma pulse, and plasma purge were 3.12, 5, 5, and 5 s, respectively. Various bias voltages up to −50 V were applied to the substrate electrode during the complete duration (5 s) of the plasma pulse. The matching network for the substrate electrode was set to an automatic mode; hence, the power varied automatically to keep the bias voltage to the set value. The reactor was initially pumped to a base pressure of 0.02 Pa. After setting the gas flows, the reactor reaches the operating pressure of 3 Pa. The results are compared with the $HfO_2$ deposited in the FlexAL system (see Figure 1b) using tris(dimethylamino)cyclopentadienyl hafnium (TDMACpH) and oxygen plasma at a 150 °C deposition temperature.[13] The deposition parameters are summarized in Table 1.

**High-Reflective Mirror.** Several high-reflective (HR) mirrors have been deposited at 100 °C using $HfO_2$ and $SiO_2$ as high (H) and low refractive (L) index materials, respectively. The deposition conditions for the $SiO_2$ layers are given elsewhere.[31] The deposition was performed on 25 mm diameter fused silica substrates of 1 mm thickness, fused silica substrates of dimension 25 mm × 25 mm ×


https://doi.org/10.1021/acsami.1c21889
ACS Appl. Mater. Interfaces 2022, 14, 14677−14692

**Table 1. Process Parameters of the $HfO_2$ Deposited in the SILAYO and the FlexAL Systems**

| process parameters | SILAYO | FlexAL |
|---|---|---|
| precursor | TDMAH | TDMACpH |
| precursor temperature | 50 °C | 60 °C |
| precursor delivery type | bubbler mode | bubbler mode |
| deposition temperature | 100 °C | 150 °C |
| ICP power | 100 W | 400 W |
| $O_2$ flow | 200 sccm | 100 sccm |
| Ar flow | 160 sccm | 100 sccm |
| operating pressure | ≈3 Pa | ≈2 Pa |
| precursor pulse | 3120 ms | 400 ms |
| precursor purge | 5000 ms | 2000 ms |
| plasma pulse | 5000 ms | 8000 ms |
| substrate biasing[a] | 5000 ms | 8000 ms |
| plasma purge | 5000 ms | 3000 ms |

[a]Substrate biasing was applied during the entire duration of the plasma pulse.

3.05 mm provided by Layertec GmbH, a double side polished (DSP) 76 mm diameter c-Si(100) wafer, and 50 mm diameter aspherical lenses (BK7) of 25 mm height. The HR design consists of quarter-wave stacks (LH)[15]. Here, we report the detailed optical performance of a mirror with the highest reflectance value at 532 nm wavelength.

**Characterization Techniques.** *Ellipsometry.* The thickness and refractive index of the $HfO_2$ films deposited on c-Si substrates were determined using the SE850 DUV spectroscopic ellipsometer (SE) (Sentech Instruments GmbH, Berlin, Germany). The films were measured in the spectral range of 200−980 nm at 75° angle of incidence (AOI). The curve fitting was performed using an optical model consisting of a c-Si substrate, 1.5 nm native oxide layer, $HfO_2$ thin film, and an effective medium approximation (EMA) layer with 50% void to account for the coating surface roughness. The optical properties of the $HfO_2$ were parametrized with a Tauc−Lorentz model with three oscillators.[27]

*X-ray Reflectometry (XRR) and X-ray Diffraction (XRD).* The density and surface roughness of the $HfO_2$ films deposited on c-Si substrates were determined by X-ray reflectometry (XRR). Therefore, a D8 Discover (Bruker AXS, Karlsruhe, Germany) diffractometer in Bragg−Brentano geometry with Cu K$\alpha$ radiation (wavelength of 0.154 nm), 40 kV acceleration voltage, and 40 mA cathode current was used. XRR data were analyzed using the Leptos 7 software package (Bruker AXS, Karlsruhe, Germany). The X-ray diffraction (XRD) measurements to determine the crystalline structure within the $HfO_2$ thin films were performed with the same instrument.

*Atomic Force Microscopy (AFM).* The topography of the $HfO_2$ films was evaluated using an atomic force microscope (AFM) Dimension D3100 (Digital Instruments (now Bruker), Santa Barbara, CA). The measurements were performed in a tapping mode on a 2 × 2 $\mu m^2$ surface area of DSP c-Si samples of dimension 25 × 25 $mm^2$, and 512 × 512 data points were analyzed. The single-crystalline Si cantilever had a tip radius of 10 nm. The AFM images were processed using Nanoscope Analysis software. Additionally, AFM measurements were performed on a mirror deposited on fused silica and c-Si substrates.

*Scanning Electron Microscopy (SEM).* The microstructure of the $HfO_2$ films deposited on c-Si substrates was investigated using a Hitachi S-4800 (Hitachi, Tokyo, Japan) field emission scanning electron microscope (SEM). The acceleration voltage and working distance were 0.7 kV and 2.4 mm, respectively.

*Auger Electron Spectroscopy (AES).* Auger electron spectroscopy (AES) was performed to evaluate the stoichiometry, and carbon and nitrogen impurities in the $HfO_2$ films deposited on c-Si substrates. AES equipment (Varian Inc., Palo Alto, CA) applies an electron beam of 5 keV focused at 30° AOI. The depth profiling was executed using Kr ions with 2 keV energy and 10 $\mu$A current.

*UV−Vis Spectrophotometry.* An Olympus K. K. USPM-RU-W near-infrared (NIR) microspectrophotometer (Olympus Corporation, Tokyo, Japan) was used to measure the reflectance on the BK7 lens at different positions with a spot size of about 30 $\mu$m. The lens was placed on a tilt stage and tilted to angles up to 60°.

*Fourier Transform Infrared (FTIR) Spectroscopy.* The relative content of residual hydroxyl groups within the $HfO_2$ films was assessed from absorbance spectra obtained by Fourier transform infrared (FTIR) spectroscopy (Varian Inc., Palo Alto, CA). The IR transmission measurements were recorded from $HfO_2$ films deposited on DSP Si wafers of a 75 mm diameter in a spectral range of 400−4000 $cm^{-1}$.

*Mechanical Stress.* The residual stress in the films was estimated from the deviation in the curvature of a 75 mm diameter (400 $\mu$m thickness) DSP wafer before and after deposition. The measurements were performed at room temperature using a Tencor FLX-2320 system (KLA-Tencor, San Jose). The residual stress is calculated using Stoney's equation given by

$$\sigma = \frac{1}{6}\frac{E_s}{(1-\vartheta_s)}\left(\frac{1}{R_f}-\frac{1}{R_s}\right)\frac{t_s^2}{t_f} \quad (1)$$

where $E_s$ is the Young's modulus, $\vartheta_s$ is the Poisson's ratio of the substrate, $R_s$ and $R_f$ are the radii of curvature of the substrate before and after coating, and $t_s$ and $t_f$ are the thickness of the substrate and the film, respectively.

*Cavity Ring-Down (CRD) Spectroscopy.* Cavity ring-down (CRD) spectroscopy was used for a precise determination of the reflectance

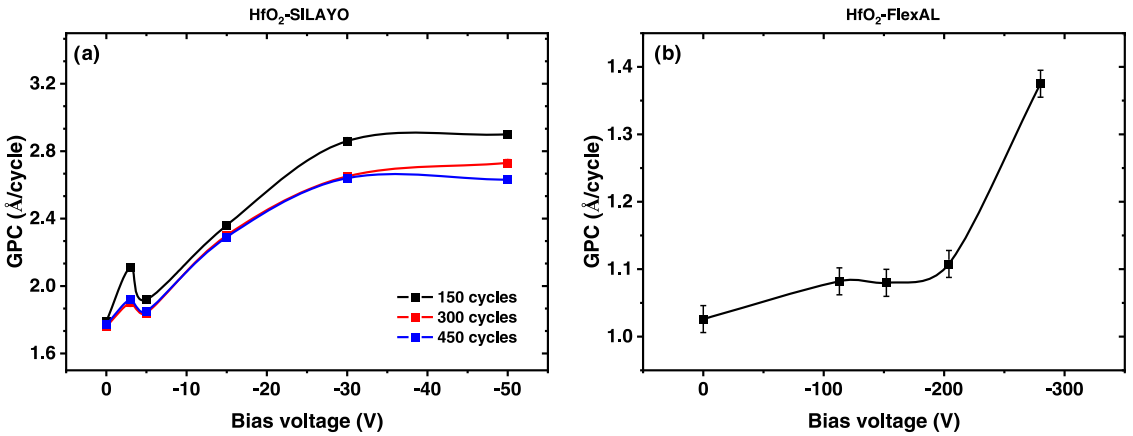


**Figure 2.** Variation in growth per cycle (GPC) of $HfO_2$ deposited by varying the bias voltage in the (a) SILAYO system at 100 °C with varying ALD cycles and (b) the FlexAL system at 150 °C.


https://doi.org/10.1021/acsami.1c21889
ACS Appl. Mater. Interfaces 2022, 14, 14677−14692

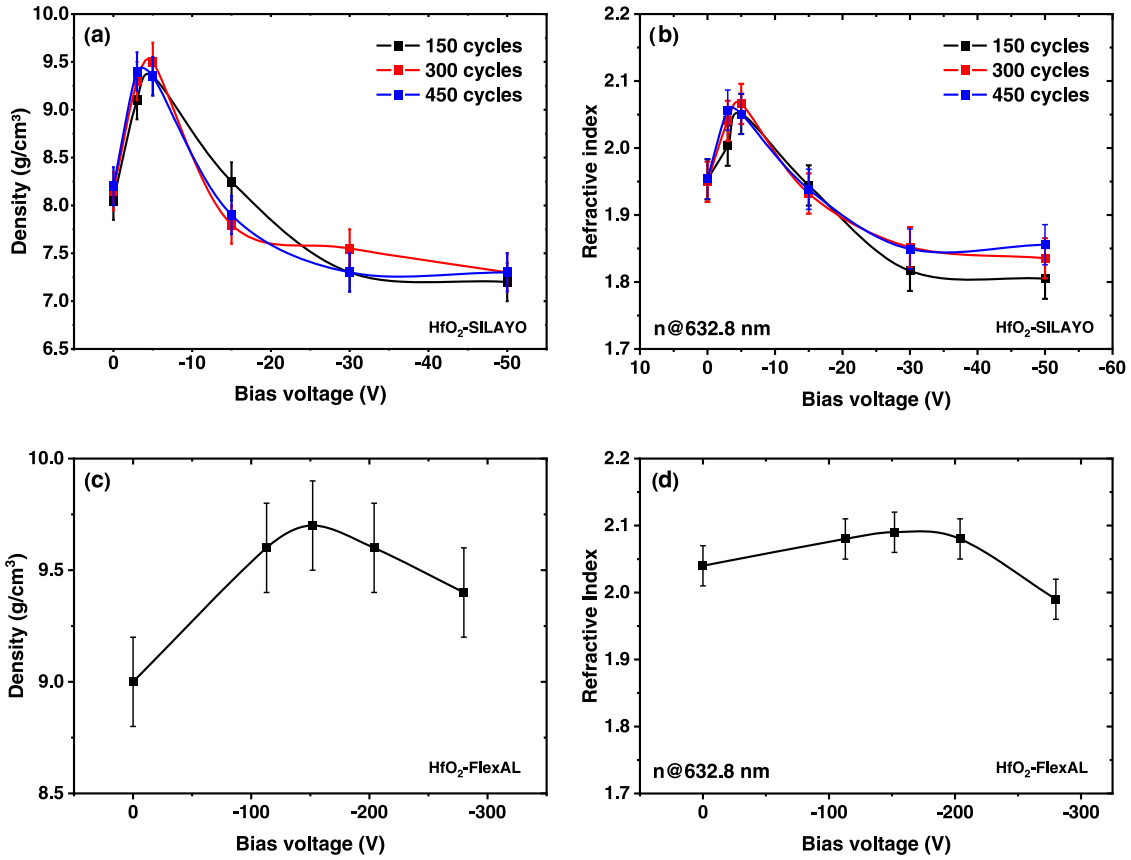


**Figure 3.** Variation in density and refractive index ($n$ at 632.8 nm) with the bias voltage for the $HfO_2$ films deposited in the (a, b) SILAYO system at 100 °C with varying ALD cycles and in the (c, d) FlexAL system at 150 °C.

of the mirrors at 355 and 532 nm, respectively.[79,80] The measurement was performed on the mirrors deposited on the fused silica substrates of dimension 25 mm × 25 mm × 3.05 mm using Layertec's custom-built CRD setup. Therefore, a pulse from an EKSPLA NT242 SH +SFG OPO is coupled into an optical cavity consisting of two highly reflecting mirrors. While circulating in the cavity, the pulse intensity $I(t)$ decreases with every round trip. This intensity loss depends on the reflectance of the cavity mirrors. A photodetector behind the cavity measures the exponential intensity decay, and the time constant $\tau$ is determined from the relation $I(t) = I_0 \exp(-t/\tau)$. Then, the reflectance $R$ of the cavity mirrors, either two identical test mirrors or one test mirror and one known reference mirror, can be calculated using

$$\sqrt{R_1 R_2} = 1 - \frac{L}{c\tau} \quad (2)$$

where $L$ is the cavity length and $c$ is the speed of light.

*Photothermal Common-Path Interferometry (PCI).* Absorption losses of the mirror deposited on fused silica were measured at 532 nm by photothermal common-path interferometry (PCI) using a custom-built setup of Layertec GmbH. Details on the setup are given elsewhere.[27] The details on the absorption measurement using a laser-induced deflection (LID) technique, scattering measurement, and laser-induced damage threshold (LIDT) at 532 nm wavelength are given in the Supporting Information.

*Environmental Stability.* The environmental stability of the mirrors was evaluated according to ISO 9221-4 norm. A climate test was performed for 48 h at 85 °C and 85% relative humidity. After the climate test, the adhesion of the mirror was evaluated by performing tape and cross-hatch tests.

## RESULTS AND DISCUSSION

**$HfO_2$ Single Layers.** The growth characteristics of $HfO_2$ thin films deposited in the SILAYO and the FlexAL system at different process conditions (Table 1) are shown in Figure 2. The growth per cycle (GPC) of $HfO_2$ films deposited without bias in the SILAYO system is ~1.77 ± 0.02 Å/cycle and in the FlexAL system is 1.03 ± 0.02 Å/cycle. The GPC of the $HfO_2$ films deposited without bias in the SILAYO system is high compared to the literature values (0.7−1.7 Å/cycle).[14,25] Jung et al. has shown that the addition of Ar into the oxygen plasma increased GPC of $HfO_2$ films by 44% compared to the film deposited with only oxygen plasma.[28,81] However, further in-depth investigation is required to understand the effect of process parameters on plasma species and ion energies in the SILAYO system.

The significant difference in GPC of the films deposited without bias in the SILAYO and the FlexAL system stems from a difference in precursors and deposition temperatures (see Table 1). Park et al. compared the GPC of $HfO_2$ deposited with TDMAH and TDMACpH as organometallic precursors and ozone as the oxygen source.[82] They reported significantly higher GPC of $HfO_2$ thin films deposited at low deposition temperature with TDMAH than films deposited with TDMACpH precursors. A high GPC can also be due to high-density plasma generated due to the uniquely designed planar triple spiral antenna (PTSA) inductively coupled plasma (ICP) source of the SILAYO system.[27,83] On increasing bias voltage, the $HfO_2$ deposited in the SILAYO system shows a three-stage behavior. Initially, on increasing the substrate bias to −3 V, the GPC increases slightly. This GPC increase can be


https://doi.org/10.1021/acsami.1c21889
ACS Appl. Mater. Interfaces 2022, 14, 14677−14692

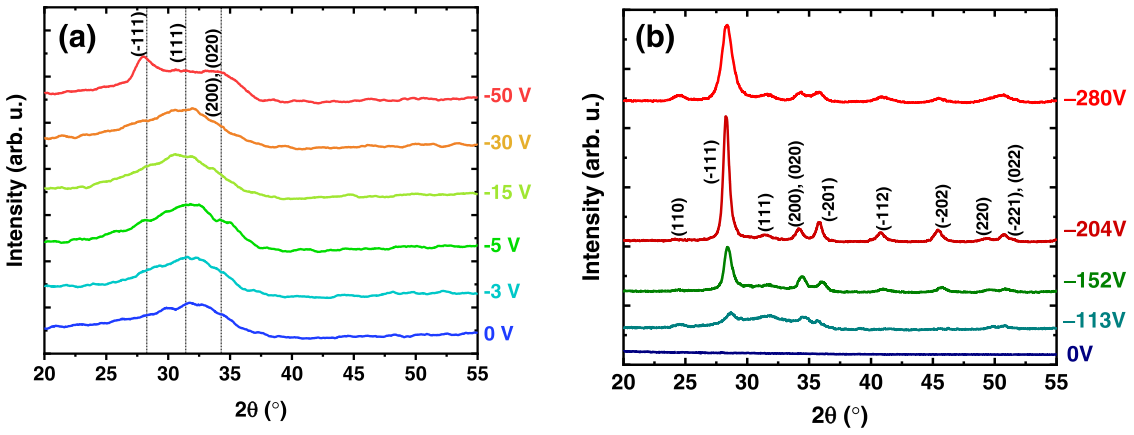


**Figure 4.** XRD diffractograms of $HfO_2$ deposited at the various bias voltage in the (a) SILAYO system (450 cycles) at 100 °C and (b) GIXRD diffractograms of the film growth in the FlexAL system at 150 °C.

due to a change in the microstructure of the $HfO_2$ films and surface functional groups involved in the reactions. On further increasing bias voltage to −5 V, the GPC decreases. Applying a bias higher than −5 V, the GPC increases again and remains relatively stable for $HfO_2$ films deposited using −30 to −50 V biases. The relatively high GPC at a higher negative bias voltage can be due to less dense films with a porous microstructure.[14,84,85]

The $HfO_2$ films deposited in the FlexAL system show a two-stage behavior.[13] The GPC increases linearly on increasing biasing up to −204 V. The GPC increases significantly to 1.38 ± 0.02 Å/cycle on further increasing the bias voltage to −280 V. The change in the growth characteristics of $HfO_2$ films on applying substrate biasing indicates a microstructure evolution with the assistance of energetic ions.

The effect of a substrate bias on the density of $HfO_2$ films is shown in Figure 3a,c. The densities of $HfO_2$ films deposited without bias with 150, 300, and 450 cycles in the SILAYO system are 8.2 ± 0.2 g/cm$^2$. The low density of the films compared to bulk (9.7 g/cm$^3$) indicates amorphous films. Increasing the bias voltage to −5 V, the densities increase and reach a maximum value of 9.4 ± 0.2 g/cm$^3$, which is close to the bulk density[86,87] and comparable to $HfO_2$ deposited by PVD techniques, like ion beam sputtering, ion-assisted deposition, and plasma ion-assisted deposition with Xe as working gas or ion plating.[88] For a bias voltage higher than −5 V, the densities of $HfO_2$ films decrease significantly and reach the minimum values of 7.2 ± 0.2 g/cm$^3$ at −50 V bias voltage. This indicates a deterioration in the film morphology under intense ion bombardment.[23] Interestingly, although there is a profound effect of substrate biasing on the density of the $HfO_2$ films, the density remains nearly constant with the increasing film thickness (increasing ALD cycles).

Similar behavior is observed in the $HfO_2$ films deposited in the FlexAL system.[13] The $HfO_2$ films deposited without bias show a density of 9.0 ± 0.2 g/cm$^3$. By increasing the bias voltage to −152 V, the density reaches a maximum value of 9.7 ± 0.2 g/cm$^3$, which is approximately the bulk density of $HfO_2$.[86,87] By increasing the bias voltage further to −280 V, the density decreases to 9.4 ± 0.2 g/cm$^3$. Thus, by applying a substrate bias, the film density can be increased significantly at low temperatures (100 °C in the SILAYO and 150 °C in the FlexAL systems). However, the application of higher substrate bias voltages leads to less dense films indicating a void-rich microstructure.[23]

The variation in the refractive index of $HfO_2$ deposited in the SILAYO and the FlexAL systems correlates with the film density profiles as shown in Figure 3b,d. The $HfO_2$ films deposited without bias in the SILAYO system show a refractive index of 1.95 ± 0.03 at 632.8 nm, independent of the film thickness. The refractive index increases to a maximum value of 2.06 ± 0.03 for all $HfO_2$ films when a bias voltage of −5 V is applied. This is in agreement with the increasing density of $HfO_2$ films deposited at −5 V bias. By increasing the bias voltage to −50 V, the lowest refractive index is observed, probably due to the formation of voids due to energetic ion bombardment.[23,89] The dispersion spectra shown in Figure S5a−c in the Supporting Information present a similar trend in the broad spectral range from 200 to 980 nm. Increasing the refractive index with increasing bias voltage is more prominent in the wavelength range above the absorption edge (230 nm).

A similar effect is also observed for $HfO_2$ deposited in the FlexAL system. A refractive index of 2.04 ± 0.03 is determined for films deposited without bias. Applying a −152 V bias, the refractive index peaks at 2.09 ± 0.03, indicating film densification. However, increasing the bias further, the refractive index decreases linearly, signifying an increase in the void content due to the bombardment with high-energy ions. The increase in density and refractive index of $HfO_2$ films with increasing temperature is reported in several studies.[14,27,70,84] A slightly higher density and refractive index of $HfO_2$ films deposited in the FlexAL system compared to the SILAYO system can be due to the higher deposition temperature (150 °C).

The effect of a substrate bias on the extinction coefficient of $HfO_2$ films deposited in the SILAYO system is shown in Figure S5d−f in the Supporting Information. A low extinction coefficient (for $\lambda$ > 230 nm) is observed for films deposited without bias and −5 V bias (in films deposited with 150 and 300 cycles). A high extinction coefficient close to the absorption edge (>250 nm) is observed on applying a bias voltage higher than −5 V, indicating more defects and absorbing impurities incorporated in the films. In the films deposited with 450 cycles and substrate biasing, the extinction coefficient increases already below 450 nm wavelength, indicating crystallization-induced defects. An increase in absorption at 532 nm wavelength with an increase in crystallization was reported earlier.[27]

The change in the microstructure with substrate biasing is presented in the X-ray diffractograms in Figure 4. The $HfO_2$


https://doi.org/10.1021/acsami.1c21889
ACS Appl. Mater. Interfaces 2022, 14, 14677−14692

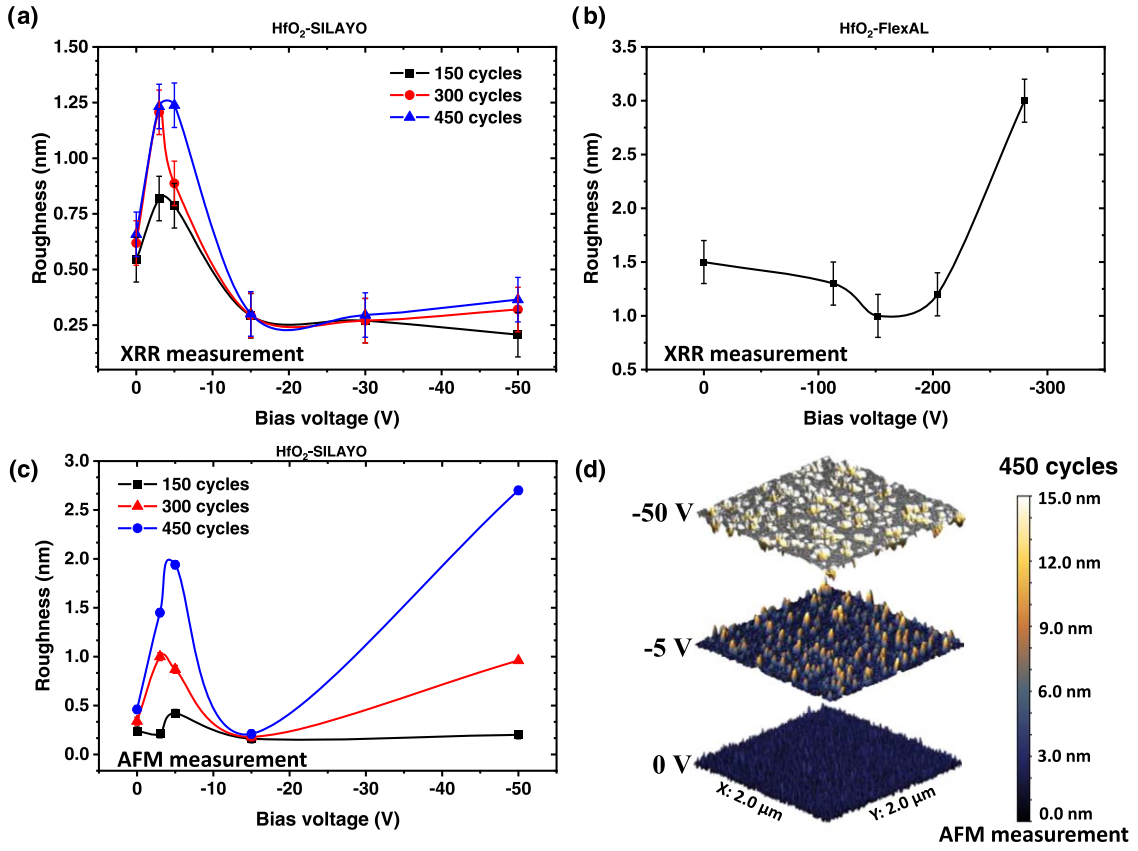


**Figure 5.** Variation in root mean square (RMS) roughness and surface morphology of $HfO_2$ films deposited by varying the bias voltage measured by (a, b) XRR and (c, d) AFM. The films were deposited in the SILAYO system (a, c, d) at 100 °C with varying ALD cycles and the (b) FlexAL system at 150 °C.

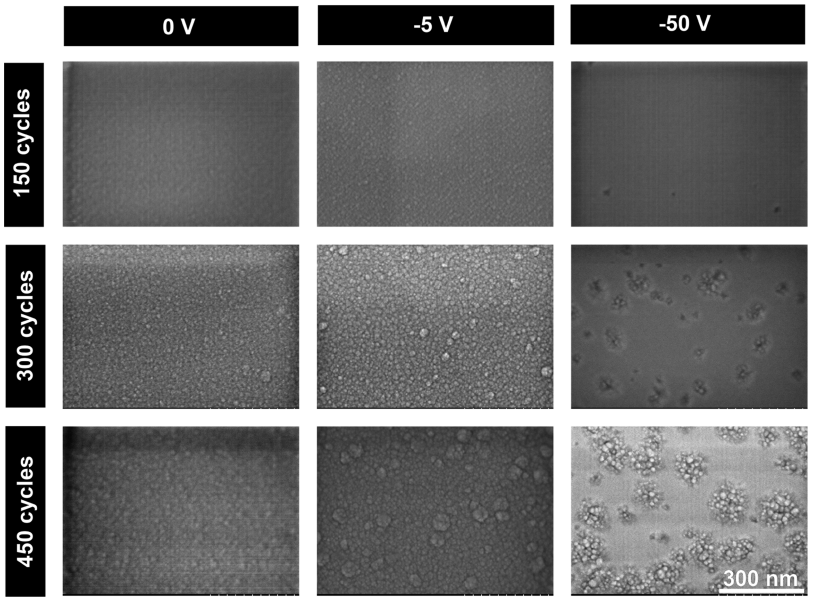


**Figure 6.** SEM images of $HfO_2$ films deposited in the SILAYO system by varying the bias voltage and a number of ALD cycles. The scale bar in the bottom right picture applies to all images.

films deposited (in the SILAYO system) without bias and with bias voltage up to −30 V show a broad peak around $2\theta \approx 32°$. On implementing −50 V bias, a broad peak in the range of 25−40° and the emergence of a sharp peak around $2\theta \approx 28°$ corresponding to the $(\bar{1}11)$ monoclinic phase[13,90] is observed. This indicates an increase in the small crystalline fraction of polycrystalline centers in an amorphous matrix of the $HfO_2$ films. In the plasma-assisted process, an increase in crystallinity is observed due to an increase in ion energies.[88,91]

A similar evolution of the microstructure with varying bias voltage is seen for the $HfO_2$ films deposited in the FlexAL system. The absence of peaks in the films deposited without


https://doi.org/10.1021/acsami.1c21889
ACS Appl. Mater. Interfaces 2022, 14, 14677−14692

bias indicates an amorphous microstructure. A fairly broad peak around 25−40° is observed when −113 V is applied, indicating films with higher crystalline incorporation into the amorphous matrix. For the films deposited using −204 V, the monoclinic peaks become more prominent due to a polycrystalline film formation. A broad peak is observed with −280 V, indicating small crystallites.[13,40,92−94]

The change in the morphology of $HfO_2$ films on applying substrate biasing is also evident in the surface roughness measured using XRR and AFM. The surface roughness determined by XRR (see Figure S6 in Supporting Information) of the $HfO_2$ films deposited in the SILAYO system is shown in Figure 5a. The films deposited without bias show a low surface roughness confirmed by a smooth surface in the three-dimensional (3D) AFM image of the film deposited with 450 cycles shown in Figure 5d. The XRR and AFM measurements shown in Figure 5a,c show the maximum value of the surface roughness at the application of −5 V bias voltage. The hillocks formation contributes to increased roughness,[14] as evident in the SEM analysis discussed in the next section (see Figure 6). When the highest bias voltage of −50 V is applied, the roughness increases significantly, as observed in AFM images (Figure 5c). Contrary to XRR, the AFM measurements show a significant increase in roughness when −50 V bias voltage is applied. The high roughness could be due to the difference in spatial frequency for a highly rough surface and non-Gaussian roughness distribution.[95] A similar trend of void formation with high-energy ions was reported by Iwashita et al. for $TiO_2$ films deposited using substrate biasing in PEALD.[89] They observed that at each oxidation step, the amorphous film consists of cleavages as a consequence of high-energy ion bombardment. The commutative ion bombardments result in the formation of fine pores in the films. It is important to mention that the fraction of high energetic ions present in the ion energy distribution (IED) could also contribute to the sputtering or void formation in the films.[13,89]

The evolution of the surface roughness with substrate biasing also strongly depends on the film thickness. Nie et al. have shown that the thin films are amorphous at the initial growth stage and crystallize when the film thickness exceeds a critical value.[96] At a given temperature, the difference in the bulk Gibbs free energy of the amorphous and crystalline states increases linearly with thickness. Crystallization may occur when the negative bulk energy difference between the amorphous and crystalline states is compensated with the positive change in the interface and surface free energies.[96] The thermal fluctuations during high deposition temperatures or postdeposition annealing drive crystallization in the film growth by lowering the activation barrier.

A similar trend in the surface roughness with increasing bias voltage in $HfO_2$ films deposited in the FlexAL system is shown in Figure 5b. The films deposited with −152 V bias are smoother compared to films deposited without bias. The increase in mobility of surface species induced by energetic ions during the film growth can result in coalescence at the grain boundary leading to a smooth surface. The significant increase in the surface roughness at high bias is due to void formation under intense ion bombardment.[13,40,92−94]

The SEM images (see Figure 6) of $HfO_2$ films deposited in the SILAYO system show a clearer picture of the change in surface morphology on applying substrate biasing. The $HfO_2$ films deposited without bias show a smooth surface with a slightly rougher texture of thick $HfO_2$ films deposited with 300 and 450 cycles. The $HfO_2$ film deposited using 150 cycles and −5 V bias voltage also appears to be slightly rougher than the film deposited without bias. However, the initiation of crystallization is seen when a bias voltage of −5 V is applied for $HfO_2$ films deposited using 300 cycles. The appearance of nanocrystallites is more prominent in the thicker (450 cycles) $HfO_2$ film deposited with a −5 V bias. The thin $HfO_2$ film deposited using the bias voltage of −50 V shows defects due to the high energy of ions impinging on the surface. With increasing thickness, clusters of nanocrystallites with voids in the center are observed for the $HfO_2$ film deposited with 300 cycles and −50 V bias. These clusters and voids become more pronounced in the thicker $HfO_2$ film (450 cycles) deposited using a −50 V bias.

The effect of substrate biasing on the residual OH groups in the $HfO_2$ films deposited in the SILAYO system is shown in the FTIR spectra (normalized thickness) (Figure 7a−c). A

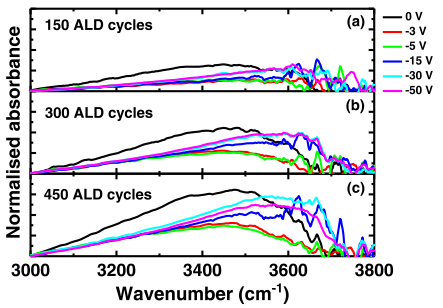


**Figure 7.** Infrared absorption spectra (normalized thickness) of $HfO_2$ deposited by varying bias voltage in the SILAYO system with (a) 150 cycles, (b) 300 cycles, and (c) 450 cycles.

broad peak in the range of 3000−3800 $cm^{-1}$ corresponding to residual OH groups is observed for the $HfO_2$ films deposited without bias.[70] A significant decrease in the residual OH content is observed for $HfO_2$ films deposited with a −5 V bias. A significant amount of residual OH content is eliminated as a result of increased ion energies due to substrate biasing, and a significant change of the surface functional groups in the reactions is indicated. On further increasing bias voltage, the residual OH content increases, correlated with void formation and adsorption of moisture. Additionally, a shift in the absorption peak by applying bias voltage indicates a difference in the dominant −OH species (isolated −OH or vicinal −OH groups with hydrogen bridge bonding).

The impurity content and stoichiometry of thicker $HfO_2$ films (450 cycles) deposited in the SILAYO system were analyzed using AES measurements (see Table 2). The $HfO_2$ films deposited without bias show high C and N contents of 13.4 ± 2.3 and 3.3 ± 0.6%, respectively. The C and N impurities decreased significantly to 3.3 ± 0.4 and 1.2 ± 0.3%, respectively, when a bias voltage of −5 V was applied.[97] At low deposition temperatures and in the absence of substrate biasing, ligands from the metal−organic precursor can be incorporated into the films. This can result in high C and N impurities. When the bias voltage is applied, the ions of moderate energy assist enhanced ligand removal, thereby decreasing impurities and leading to densification.[45] As observed for the residual OH content, the C and N impurities increase significantly to 7.7 ± 1.0 and 3.5 ± 1.4%, respectively, when a high bias voltage of −50 V is applied. The films are slightly oxygen-rich with an O/Hf ratio of 2.2 ± 0.1.


https://doi.org/10.1021/acsami.1c21889
ACS Appl. Mater. Interfaces 2022, 14, 14677−14692

Table 2. Atomic Concentrations of $HfO_2$ Thin Films Deposited with 450 Cycles Determined by Auger Electron Spectroscopy

| bias voltage (V) | Hf (%) | C (%) | N (%) | O (%) | O/Hf |
|---|---|---|---|---|---|
| 0 | 24.9 ± 0.8 | 13.4 ± 2.3 | 3.3 ± 0.6 | 58.4 ± 2.9 | 2.3 ± 0.1 |
| −3 | 29.9 ± 1.0 | 3.9 ± 0.5 | 1.2 ± 0.2 | 65.1 ± 1.3 | 2.2 ± 0.1 |
| −5 | 29.2 ± 0.8 | 3.3 ± 0.4 | 1.2 ± 0.3 | 66.2 ± 0.4 | 2.3 ± 0.1 |
| −15 | 27.9 ± 1.3 | 4.5 ± 0.7 | 2.3 ± 0.3 | 65.1 ± 1.1 | 2.3 ± 0.2 |
| −50 | 27.9 ± 0.9 | 7.7 ± 1.0 | 3.5 ± 1.4 | 58.4 ± 2.9 | 2.1 ± 0.1 |

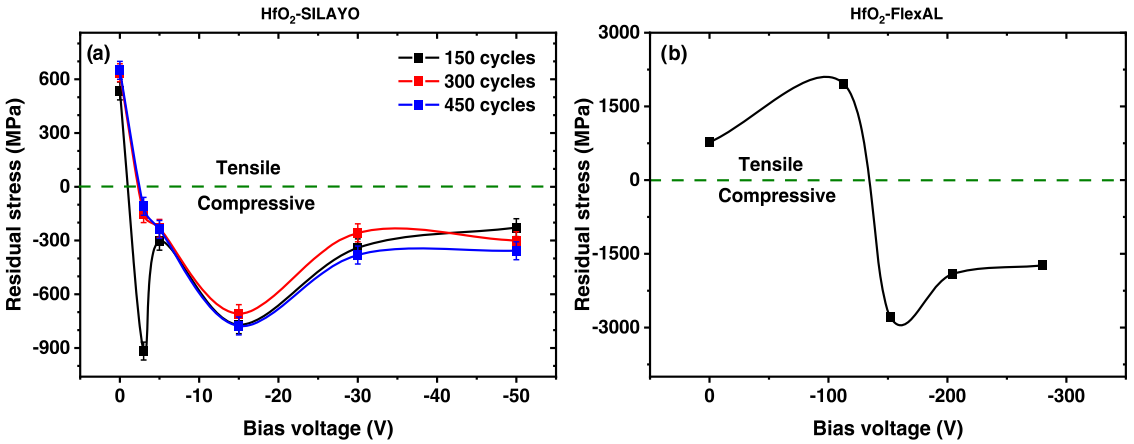


**Figure 8.** Variation in residual stress of $HfO_2$ deposited by varying the bias voltage in the (a) SILAYO system at 100 °C with varying ALD cycles and the (b) FlexAL system at 150 °C.

The effect of substrate biasing on the residual stress of $HfO_2$ thin films was also investigated. Figure 8a depicts the residual stress in $HfO_2$ films deposited in the SILAYO system. The $HfO_2$ films deposited without bias using 150, 300, and 450 cycles show tensile stress of 535, 635, and 650 ± 50 MPa, respectively. The intrinsic residual stress in the thin films results from several competing mechanisms arising from OH incorporation, impurities, voids, crystallization, and film thickness.[71,98−100] The $HfO_2$ films deposited with varying deposition temperature, thickness, postdeposition annealing temperature, and without energetic ions assistance are under tensile stress, typically observed in the materials with low atomic mobility.[70,71,100] The tensile stress in films deposited without bias is due to attractive forces within atomic-size pores.[71]

For thin $HfO_2$ films deposited using 150, 300, and 450 cycles, the residual stress changes to compressive on applying a bias voltage of −3 V. The films of low atomic mobility materials transit from tensile to compressive stress subjected to energetic ions.[71] When the energies of the arriving particles are higher than the energy threshold for atomic displacement, it induces displacement of subsurface atoms located at the impact site to more favorable sites, such as vacant sites, accompanied by film densification, as evident in Figure 3a,c.

The peak compressive stress is observed already at −3 V bias for the thin film (150 cycles) compared to thick films (300 and 450 cycles), demonstrating that the interface between the film and the substrate is the dominant factor for stress formation in thinner films.[71] The measured stress at −3 V is reliable, as repeated deposition and analysis showed a consistent result. The compressive stress of thinner films decreases to values similar to thicker films on applying a bias voltage of −5 V, probably due to the film thickness reaching the value where the effect of the substrate−film interface is not dominant any longer.

High compressive stress is observed when a bias voltage of −15 V is applied, whereas stress relaxation occurs at −30 V.[71] The stress relaxation at high ion energies is the balance between implantation and relaxation.[71,101] The implanted atoms tend to move to the surface to release stress in the film but are hindered by the repulsive forces of neighboring atoms. Thus, these atoms are in a metastable position near the surface of the film. With ion bombardment, a fraction of the incoming ion energy is transferred to these implanted atoms removing them from the metastable position to a stable position by thermal spiking.[71,101] For all $HfO_2$ films, the compressive stress remained nearly constant on further increasing the bias voltage to −50 V. The low stress at −50 V bias is due to the formation of voids and defects as the high ion energy leads to thermal spikes and knock-on implantation of plasma species.[45,46,71,102]

For the $HfO_2$ films deposited in the FlexAL system (Figure 8b), the mechanical stress increases up to 2000 ± 50 MPa tensile stress values and becomes compressive up to −3000 ± 50 MPa on the application of a bias voltage of −113 and −152 V, respectively. The stress relaxation in the void-rich microstructure of films due to ion-induced damage at a higher bias voltage is also observed. Bias voltage values resulting in near-zero stress are possible for both systems, which is important to deposit mechanically stable films.

Therefore, applying substrate biasing can significantly improve material properties, resulting in dense films with a high refractive index, crystalline microstructure, low residual OH impurities, and low C and N impurities. The change in mechanical stress from compressive to tensile on applying substrate biasing is further advantageous in depositing high-reflective mirrors, filters, and beamsplitters with numerous layers. Several high-reflective (HR) multilayer mirrors at 355 and 532 nm wavelengths were deposited, but the mirrors at 532 nm were thoroughly characterized and will be discussed in detail.


https://doi.org/10.1021/acsami.1c21889
ACS Appl. Mater. Interfaces 2022, 14, 14677−14692

**HR Mirror at 532 nm.** The PEALD mirrors were deposited without and with several substrate bias conditions. The bias voltage was kept low, with values only up to −15 V. All mirrors grown without bias show cracks due to a high mechanical stress indicating that substrate biasing is essential toward complex optical functional coatings, but no crack formation is observed with biasing conditions.

Using cavity ring-down (CRD) spectroscopy,[80,103] it was found that the mirrors deposited here exhibit a reflectance up to 99.93% at 532 nm (see Figure 9). High reflectance values of

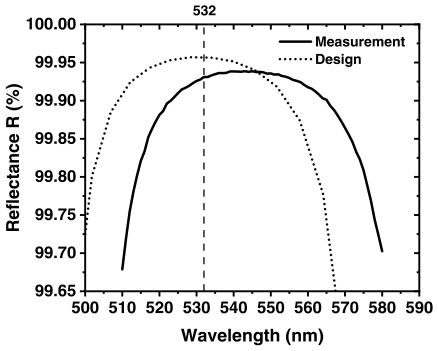


**Figure 9.** Reflectance of the mirror by cavity ring-down spectroscopy at 532 nm.

above 99.9% have also been obtained for mirrors at 355 nm wavelength. The properties of a mirror at 532 nm are summarized in Table 3. The measured reflectance spectra are

**Table 3. Summary of Results Obtained for a PEALD Mirror at 532 nm**

| parameter/measurement technique | result |
|---|---|
| calculated thickness | 2.3 $\mu$m |
| total stress | 120 ± 50 MPa (tensile) |
| reflectance (CRD) | 0.9993 |
| absorbance (ppm) (PCI) | 10.8 ± 3.8 |
| absorbance (ppm) (LID) | 5.8 ± 1.3 |
| total scattering (ppm) | 4 ± 1.2 |
| residual transmittance (ppm) | 530 ± 50 |
| energy budget (R + T + S + A) (ppm) | 999 845 ± 55 |
| scatter relevant roughness (nm) WLI | ~0.5 nm |
| LIDT (R-on-1) HR | 19 ± 4 J/cm$^2$ |
| LIDT (R-on-1) substrate | 154 ± 34 J/cm$^2$ |
| LIDT (1000-on-1 ramp) HR | 80 ± 18 J/cm$^2$ |
| LIDT (10 000-on-1 ramp) substrate | 142 ± 33 J/cm$^2$ |

slightly shifted to higher wavelengths compared to the theoretical design due to a deviation of the film thickness from the target. The film thicknesses have been reached from known growth rate values without in situ monitoring and control. The reflectance measured on an aspherical lens with a microspectrophotometer (USPM) also shows some shift of the reflectance peak position because of film thickness variations across the reactor (see Figure S7 in the Supporting Information). The thickness deviation over the lens surface can be further improved by process optimization to improve the uniformity in the height of the reactor for coating complex-shaped optics.

Precise measurements of optical losses in the form of absorption and scattering are necessary for high-performance optics. The absorption measurement of the mirrors at 355 and 532 nm wavelengths using the photothermal common-path interferometry (PCI) method results in 57 ± 3.8 ppm and 10.8 ± 3.8 ppm, respectively. Additionally, the absorption at 532 nm has also been measured using laser-induced deflection (LID), which yielded 5.8 ± 1.3 ppm, in good agreement with the PCI value. The difference between the absorption measured by PCI and LID likely originates from the different calibration procedures.

The sources of absorption in the coating can be intrinsic, such as defects in the form of impurities, nonstoichiometric defects in the form of oxygen vacancies,[54] and extrinsic defects like inclusions in the form of nodules.[104,105] The shallow oxygen vacancy-related absorbing defects in $HfO_2$ are located a few eV below the conduction band.[106,107] Also, there can be a small nonlinear absorption hidden by a strong linear absorption under intense laser irradiation.[108] An enlarged nonlinear absorption can result in two-photon absorption via intermediate defect levels. Since the optical band gap of $SiO_2$ is larger than $HfO_2$, $HfO_2$ should be the major contributor to nonlinear absorption in the multilayer $HfO_2/SiO_2$ mirror.[108] The nonstoichiometric defects might decrease by annealing the films, which improves stoichiometry; however, an appropriate annealing temperature should be used as the annealing-induced crystallization can also increase scattering losses. The atomic impurities in the films can be reduced using high purity precursors and optimized process conditions to prevent the incorporation of residual precursors and by-products into the films.

Film defects are also created by particles either from handling or during the film growth. Overcoating these particles or seeds creates nodular defects.[105,109] When the coating is irradiated with a monochromatic laser, it results in a standing wave because of the interference nature of the multilayer mirror. This electric field is perturbed by the nodular defects where it is enhanced significantly compared to a planar quarter-wave stack.[105] The local electric field enhancement depends on the size, depth, and absorbing inclusion within the nodules. The nodules might act as both microlenses focusing light from the outside of the angular mirror bandwidth and as micromirrors limited by reflected light within the angular bandwidth.[105,110] The nodular defects can partially be mitigated by ensuring a clean environment to avoid contaminations and by optimizing the process conditions. Monitoring and reducing contaminations also become mandatory for high-performance optics.

The optical losses of the functional coatings also have contributions from scattering. Hence, the scattering losses of the mirror were determined in transmission and reflection to 0.75 ± 0.2 and 3.3 ± 1.0 ppm, respectively (see Figure S8 in the Supporting Information). The scattering losses originate from the interface roughness and the surface of the mirror. The surface roughness was evaluated by white light interferometry (WLI) and atomic force microscopy (AFM). The root mean square (RMS) roughness of the mirror was 0.64 nm with WLI, almost identical to the substrate roughness with 0.58 nm (see Figure S9 in the Supporting Information). This was confirmed by AFM with a surface roughness of 0.51 and 0.63 nm for the mirror and substrate, respectively (see Figure S10 in the Supporting Information). The residual transmittance was additionally determined as 530 ± 50 ppm, indicating that even higher reflectance values might be obtained by increasing the number of multilayers.


https://doi.org/10.1021/acsami.1c21889
ACS Appl. Mater. Interfaces 2022, 14, 14677−14692

Impurities, nonstoichiometric defects, and microsize nodular defects mentioned above impact the laser-induced damage threshold (LIDT) in nanosecond pulse duration.[54,68,104,105] Absorption of laser radiation by these defects can result in excess local thermal energy. When the temperature reaches the melting point of the defects, evaporation and melting can occur, thereby lowering the LIDT.[54] The R-on-1 (constant number of sites irradiated with multiple laser pulse per site with the same fluence and predefined pulse energy) LIDT values of the PEALD mirrors were 19 ± 4 J/cm$^2$ (Layertec, 10 pulses/fluence) and 21.4 ± 4.9 J/cm$^2$ (RhySearch, 1000 pulses/fluence) for defect-driven onset (see Figure S11a,b in the Supporting Information). Ideal defect-free coatings can be estimated to withstand fluences of 60 ± 13 J/cm$^2$ (10 pulses/fluence) to 80 ± 18 J/cm$^2$ (1000 pulses/fluence) since only single defect sites had a low LIDT value in both measurements. The defect-driven and defect-free laser damage morphology after 1000 pulses/fluence irradiation is shown in Figure S11c,d in the Supporting Information.

Ma et al. tested the LIDT (3 ns, 10 Hz, 100 $\mu$m beam diameter) of mirrors for a 45° angle of incidence deposited using reactive e-beam evaporation using four popular methods: 1-on-1 (the constant number of sites irradiated with single laser pulse per site with predefined pulse energy), S-on-1 (the constant number of sites irradiated with multiple laser pulse per site with the same fluence and predefined pulse energy), R-on-1, and raster scan (the sample area is divided into a number of sites with diameter proportional to the beam diameter of laser).[68] They showed a resulting LIDT of 10 ± 2 J/cm$^2$ when the 1000-on-1 test was used. The R-on-1 test showed 100% LIDT of 64 ± 2 J/cm$^2$ and an average LIDT of 45.5 J/cm$^2$. The 2020 SPIE laser damage symposium surveyed state-of-the-art reflectors designed for 532 nm wavelength.[58] These mirrors deposited with five different PVD techniques were tested for LIDT using the raster scan mode (6 ns pulse duration, 100 Hz in a single-longitudinal mode). The highest LIDT of 28 J/cm$^2$ was observed for the mirror consisting of $HfO_2/SiO_2$ multilayers deposited using e-beam evaporation. Direct comparison of LIDT values of mirrors in this study with that in the literature is restricted due to different measurement types and setups since the LIDT also varies with the parameters like pulse duration, focal spot profile, temperature, etc.[111,112] However, the LIDT values obtained for these PEALD coatings are very promising for laser applications.

The net residual stress values of various mirrors (up to 2.33 $\mu$m film thickness) deposited on a Si substrate were below 120 ± 50 MPa tensile stress. The microscopic image in Figure S12a shows no cracks compared to a mirror with the same design deposited without bias (see Figure S12b in the Supporting Information). A tape test shows no delamination before and after the climate test for the crack-free mirrors. The cross-hatch test after the climate test showed less than 5% of the area being affected with small flakes of the coatings detached at the intersections.

## SUMMARY AND CONCLUSIONS

$HfO_2$ thin films were deposited using substrate biasing in two deposition systems, namely, the SILAYO and FlexAL tools. The film properties refractive index, mass density, crystallinity, surface roughness, elemental composition, and residual stress are influenced by applying bias during the plasma step of the ALD process. The magnitude of bias voltage at which material properties can be improved depends on the configuration of the ALD system. The $HfO_2$ film properties are in general improved by applying bias values below the ion-induced degradation regime. The film density and refractive index values are higher than in films without bias for optimum conditions but decrease with increasing bias values. The mechanical stress changes from tensile to compressive on applying bias. The surface roughness and film crystallinity also depend on the applied bias voltage. The increased density of the films correlates with a decrease in the residual OH content.

Applying high bias voltage above the ion-induced degradation threshold leads to plastic deformation of the film and a void-rich microstructure. As a consequence of the ion bombardment, the density and refractive index of the films also decrease. 3D AFM images show the formation of defects at high bias voltage. The XRD diffractograms and SEM images evidence monoclinic nanocrystals embedded in the amorphous matrix. The porous microstructure of the films at a high bias deposited in the SILAYO system was also accompanied by high OH incorporation. Hence, it is shown that the material properties of $HfO_2$ can be improved significantly when a low to moderate bias voltage is applied. The application of a high bias voltage deteriorates the film quality for optical applications.

Furthermore, the improved microstructure properties and transition from tensile to compressive stress on applying a low bias voltage were used to deposit dielectric mirrors. The optical properties and laser damage resistance of the mirror were extensively studied. A high reflectance of 0.9993, low absorption (<11 ppm), and scattering of 4 ± 1.2 ppm were observed at 532 nm wavelength. The surface roughness of ≈ 0.5 nm was confirmed by white light interferometry and AFM. The defect-driven LIDT of 19 ± 4 J/cm$^2$ (10 pulses irradiation) and 21.4 ± 4.9 J/cm$^2$ (1000 pulses irradiation) was observed. Ideal defect-free coatings can be estimated to withstand fluences in the range of 60 ± 13 J/cm$^2$ (10 pulses per fluence) to 80 ± 18 J/cm$^2$ (1000 pulses per fluence). The low residual stress of 120 ± 50 MPa ensures the absence of cracking and delamination. The mirror also shows high environmental stability. Adhesion tests as tape and cross-hatch tests performed immediately after the environmental test show no delamination. Hence, substrate biasing in PEALD processes provides a promising technique to deposit mechanically and environmentally stable dielectric mirrors with high reflectance and high laser damage resistance. These excellent properties observed for the dielectric mirror make this coating approach a promising candidate for high-power laser application.

## ASSOCIATED CONTENT

### Supporting Information

The Supporting Information is available free of charge at https://pubs.acs.org/doi/10.1021/acsami.1c21889.

General scheme of laser-induced deflection principle; a figure showing photothermal deflection signal; a figure showing illustration of the statistical analysis of the R-on-1 test (10 pulses) method; a figure showing details of the R-on-1 test (1000 pulses); a figure showing optical constants ($n$ and $k$) of the $HfO_2$ films deposited with 150, 300, and 450 ALD cycles; a figure showing XRR fitting of measurement and simulation; a figure showing reflectance spectra of a mirror (at 532 nm wavelength) across the surface of the BK7 lens measured with a microspot spectrophotometer; a figure showing angle-



https://doi.org/10.1021/acsami.1c21889
ACS Appl. Mater. Interfaces 2022, 14, 14677−14692

resolved scattering (ARS) curves of the mirror and uncoated substrate at 532 nm wavelength; a figure showing root mean square roughness of mirror and uncoated substrate measured with white light interferometry; a figure showing root mean square roughness of mirror and uncoated substrate measured with AFM; a figure showing LIDT with the R-on-1 test (10 pulses and 1000 pulses) on mirror and surface damage morphology after laser irradiation (R-on-1 test, 1000 pulses); a figure showing microscopy images of mirrors deposited with and without bias (PDF)

## AUTHOR INFORMATION


### Corresponding Author

**Adriana Szeghalmi** − *Institute of Applied Physics, Friedrich Schiller University Jena, 07745 Jena, Germany; Fraunhofer Institute for Applied Optics and Precision Engineering, 07745 Jena, Germany;* orcid.org/0000-0003-2055-2825; Email: adriana.szeghalmi@iof.fraunhofer.de

### Authors

**Vivek Beladiya** − *Institute of Applied Physics, Friedrich Schiller University Jena, 07745 Jena, Germany; Fraunhofer Institute for Applied Optics and Precision Engineering, 07745 Jena, Germany;* orcid.org/0000-0002-8094-6300

**Tahsin Faraz** − *Department of Applied Physics, Eindhoven University of Technology, 5600 MB Eindhoven, The Netherlands*

**Paul Schmitt** − *Institute of Applied Physics, Friedrich Schiller University Jena, 07745 Jena, Germany; Fraunhofer Institute for Applied Optics and Precision Engineering, 07745 Jena, Germany*

**Anne-Sophie Munser** − *Institute of Applied Physics, Friedrich Schiller University Jena, 07745 Jena, Germany; Fraunhofer Institute for Applied Optics and Precision Engineering, 07745 Jena, Germany*

**Sven Schröder** − *Fraunhofer Institute for Applied Optics and Precision Engineering, 07745 Jena, Germany*

**Sebastian Riese** − *Layertec GmbH, 99441 Mellingen, Germany*

**Christian Mühlig** − *Leibniz-Institute of Photonic Technology, 07745 Jena, Germany*

**Daniel Schachtler** − *RhySearch, 9471 Buchs, Switzerland*

**Fabian Steger** − *RhySearch, 9471 Buchs, Switzerland*

**Roelene Botha** − *RhySearch, 9471 Buchs, Switzerland*

**Felix Otto** − *Institute of Solid State Physics, Friedrich Schiller University Jena, 07743 Jena, Germany;* orcid.org/0000-0002-2327-5950

**Torsten Fritz** − *Institute of Solid State Physics, Friedrich Schiller University Jena, 07743 Jena, Germany;* orcid.org/0000-0001-6904-1909

**Christian van Helvoirt** − *Department of Applied Physics, Eindhoven University of Technology, 5600 MB Eindhoven, The Netherlands*

**Wilhelmus M. M. Kessels** − *Department of Applied Physics, Eindhoven University of Technology, 5600 MB Eindhoven, The Netherlands;* orcid.org/0000-0002-7630-8226

**Hassan Gargouri** − *Sentech Instruments GmbH, 12489 Berlin, Germany*

Complete contact information is available at: https://pubs.acs.org/10.1021/acsami.1c21889


### Notes

The authors declare no competing financial interest.

## ACKNOWLEDGMENTS

The authors thank Kevin Hanemann for several AFM measurements and analysis of the $HfO_2$ single layers, Tina Seifert for the climate test, tape test, and cross-hatch test, and Karl Scheuer for helping with AFM measurements on mirrors. We also gratefully acknowledge funding by the Deutsche Forschungsgemeinschaft (DFG, German Research Foundation)—Priority Program Fields Matter 1959/1 within the projects SZ253/2-1, the Fraunhofer Society within the Attract 066-601020 project, and Bundesministerium für Wirtschaft und Energie (ZF4309604SY8, ZF4596101SY8).

## REFERENCES


(1) Nishiyama, A. Hafnium-Based Gate Dielectric Materials. In *High Permittivity Gate Dielectric Materials*; Kar, S., Ed.; Springer Series in Advanced Microelectronics; Springer, 2013; Vol. *43*, pp 153−181.

(2) Gaskins, J. T.; Hopkins, P. E.; Merrill, D. R.; Bauers, S. R.; Hadland, E.; Johnson, D. C.; Koh, D.; Yum, J. H.; Banerjee, S.; Nordell, B. J.; Paquette, M. M.; Caruso, A. N.; Lanford, W. A.; Henry, P.; Ross, L.; Li, H.; Li, L.; French, M.; Mei, A. B.; King, S. W. Erratum: Review—Investigation and Review of the Thermal, Mechanical, Electrical, Optical, and Structural Properties of Atomic Layer Deposited High- k Dielectrics: Beryllium Oxide, Aluminum Oxide, Hafnium Oxide, and Aluminum Nitride. *ECS J. Solid State Sci. Technol.* **2018**, *7*, X3.

(3) Wilk, G. D.; Wallace, R. M.; Anthony, J. M. High-$\kappa$ Gate Dielectrics: Current Status and Materials Properties Considerations. *J. Appl. Phys.* **2001**, *89*, 5243−5275.

(4) Thielsch, R. Optical Coatings for the DUV/VUV. In *Optical Interference Coatings*; Kaiser, N.; Pulker, H. K., Eds.; Springer International Publishing, 2003; Vol. *88*, pp 257−279.

(5) Stolz, C. J.; Génin, F. Y. Laser Resistant Coatings. In *Optical Interference Coatings*; Kaiser, N.; Pulker, H. K., Eds.; Springer International Publishing, 2003; Vol. *88*, pp 309−333.

(6) Emmert, L. A.; Rudolph, W. Femtosecond Laser-Induced Damage in Dielectric Materials. *Laser-Induced Damage in Optical Materials*; CRC Press, 2014; pp 142−169.

(7) Al-Kuhaili, M. F.; Durrani, S. M. A.; Khawaja, E. E. Characterization of Hafnium Oxide Thin Films Prepared by Electron Beam Evaporation. *J. Phys. D: Appl. Phys.* **2004**, *37*, 1254.

(8) Niwa, M. Hf-Based High-k Gate Dielectric Processing. In *High Permittivity Gate Dielectric Materials*; Kar, S., Ed.; Springer Series in Advanced Microelectronics; Springer, 2013; Vol. *43*, pp 183−234.

(9) Stenzel, O.; Schürmann, M.; Wilbrandt, S.; Kaiser, N.; Tünnermann, A.; Mende, M.; Ehlers, H.; Ristau, D.; Bruns, S.; Vergöhl, M.; Riggers, W.; Bischoff, M.; Held, M. In *Optical and Mechanical Properties of Oxide UV Coatings, Prepared by PVD Techniques*, Proceedings of SPIE 8168, Advances in Optical Thin Films IV; International Society for Optics and Photonics, 2011; p 81681W.

(10) Thielsch, R.; Gatto, A.; Heber, J.; Kaiser, N. A Comparative Study of the UV Optical and Structural Properties of $SiO_2$, $Al_2O_3$, and $HfO_2$ Single Layers Deposited by Reactive Evaporation, Ion-assisted Deposition and Plasma Ion-assisted Deposition. *Thin Solid Films* **2002**, *410*, 86−93.

(11) Walawalkar, M. G.; Kottantharayil, A.; Rao, V. R. Chemical Vapor Deposition Precursors for High Dielectric Oxides: Zirconium and Hafnium Oxide. *Synth. React. Inorg., Met.-Org., Nano-Met. Chem.* **2009**, *39*, 331−340.

(12) Arts, K.; Utriainen, M.; Puurunen, R. L.; Kessels, W. M. M.; Knoops, H. C. M. Film Conformality and Extracted Recombination Probabilities of O Atoms during Plasma-Assisted Atomic Layer Deposition of $SiO_2$, $TiO_2$, $Al_2O_3$, and $HfO_2$. *J. Phys. Chem. C* **2019**, *123*, 27030−27035.

(13) Faraz, T.; Knoops, H. C. M.; Verheijen, M. A.; van Helvoirt, A. A.; Karwal, S.; Sharma, A.; Beladiya, V.; Szeghalmi, A.; Hausmann, D. M.; Henri, J.; Creatore, M.; Kessels, W. M. M. Tuning Material Properties of Oxides and Nitrides by Substrate Biasing during Plasma-Enhanced Atomic Layer Deposition on Planar and 3D Substrate Topographies. *ACS Appl. Mater. Interfaces* **2018**, *10*, 13158−13180.
(14) Sharma, A.; Longo, V.; Verheijen, M. A.; Bol, A. A.; Kessels, W. M. M. Atomic Layer Deposition of $HfO_2$ using $HfCp(NMe_2)_3$ and $O_2$ Plasma. *J. Vac. Sci. Technol., A* **2017**, *35*, No. 01B130.
(15) Cremers, V.; Puurunen, R. L.; Dendooven, J. Conformality in Atomic Layer Deposition: Current Status Overview of Analysis and Modelling. *Appl. Phys. Rev.* **2019**, *6*, No. 021302.
(16) Arts, K.; Deijkers, J. H.; Faraz, T.; Puurunen, R. L.; Kessels, W. M. M.; Knoops, H. C. M. Evidence for Low-Energy Ions Influencing Plasma-Assisted Atomic Layer Deposition of $SiO_2$: Impact on the Growth Per Cycle and Wet Etch Rate. *Appl. Phys. Lett.* **2020**, *117*, No. 031602.
(17) Arts, K.; Thepass, H.; Verheijen, M. A.; Puurunen, R. L.; Kessels, W. M. M.; Knoops, H. C. M. Impact of Ions on Film Conformality and Crystallinity during Plasma-Assisted Atomic Layer Deposition of $TiO_2$. *Chem. Mater.* **2021**, *33*, 5002.
(18) Fang, F.; Liu, M.; Chen, W.; Yang, H.; Liu, Y.; Li, X.; Hao, J.; Xu, B.; Wu, D.; Cao, K.; Lei, W.; Müller-Buschbaum, P.; Sun, X. W.; Chen, R.; Wang, K. Atomic Layer Deposition Assisted Encapsulation of Quantum Dot Luminescent Microspheres toward Display Applications. *Adv. Opt. Mater.* **2020**, *8*, No. 1902118.
(19) Devloo-Casier, K.; Geiregat, P.; Ludwig, K. F.; van Stiphout, K.; Vantomme, A.; Hens, Z.; Detavernier, C.; Dendooven, J. A Case Study of ALD Encapsulation of Quantum Dots: Embedding Supported CdSe/CdS/ZnS Quantum Dots in a ZnO Matrix. *J. Phys. Chem. C* **2016**, *120*, 18039−18045.
(20) Ghazaryan, L.; Pfeiffer, K.; Schmitt, P.; Beladiya, V.; Kund, S.; Szeghalmi, A. Atomic Layer Deposition. *digital Encyclopedia of Applied Physics*; American Cancer Society, 2003; Vol. *40*, pp 1−44.
(21) Profijt, H. B.; Potts, S. E.; van de Sanden, M. C. M.; Kessels, W. M. M. Plasma-Assisted Atomic Layer Deposition: Basics, Opportunities, and Challenges. *J. Vac. Sci. Technol., A* **2011**, *29*, No. 050801.
(22) Knoops, H. C. M.; Faraz, T.; Arts, K.; Kessels, W. M. M. Status and Prospects of Plasma-Assisted Atomic Layer Deposition. *J. Vac. Sci. Technol., A* **2019**, *37*, No. 030902.
(23) Boris, D. R.; Wheeler, V. D.; Nepal, N.; Qadri, S. B.; Walton, S. G.; Eddy, C. C. R. The Role of Plasma in Plasma-Enhanced Atomic Layer Deposition of Crystalline Films. *J. Vac. Sci. Technol., A* **2020**, *38*, No. 040801.
(24) Aarik, J.; Aidla, A.; Kiisler, A.-A.; Uustare, T.; Sammelselg, V. Influence of Substrate Temperature on Atomic Layer Growth and Properties of $HfO_2$ Thin Films. *Thin Solid Films* **1999**, *340*, 110−116.
(25) Blaschke, D.; Munnik, F.; Grenzer, J.; Rebohle, L.; Schmidt, H.; Zahn, P.; Gemming, S. A Correlation Study of Layer Growth Rate, Thickness Uniformity, Stoichiometry, and Hydrogen Impurity Level in $HfO_2$ Thin Films Grown by ALD between 100 °C and 350 °C. Applied Surface Science, 506, 144188. *Appl. Surf. Sci.* **2020**, *506*, No. 144188.
(26) Rammula, R.; Aarik, J.; Mändar, H.; Ritslaid, P.; Sammelselg, V. Atomic Layer Deposition of $HfO_2$: Effect of Structure Development on Growth Rate, Morphology and Optical Properties of Thin Films. *Appl. Surf. Sci.* **2010**, *257*, 1043−1052.
(27) Lapteva, M.; Beladiya, V.; Riese, S.; Hanke, P.; Otto, F.; Fritz, T.; Schmitt, P.; Stenzel, O.; Tünnermann, A.; Szeghalmi, A. Influence of Temperature and Plasma Parameters on the Properties of PEALD $HfO_2$. *Opt. Mater. Express* **2021**, *11*, 1918.
(28) Jung, H.; Oh, I.-K.; Yoon, C. M.; Park, B.-E.; Lee, S.; Kwon, O.; Lee, W. J.; Kwon, S.-H.; Kim, W.-H.; Kim, H. Effects of Ar Addition to $O_2$ Plasma on Plasma-Enhanced Atomic Layer Deposition of Oxide Thin Films. *ACS Appl. Mater. Interfaces* **2018**, *10*, 40286−40293.
(29) Hackley, J. C.; Gougousi, T. Properties of Atomic Layer Deposited $HfO_2$ Thin Films. *Thin Solid Films* **2009**, *517*, 6576−6583.
(30) Seo, M.; Min, Y.-S.; Kim, S. K.; Park, T. J.; Kim, J. H.; Na, K. D.; Hwang, C. S. Atomic Layer Deposition of Hafnium Oxide from Tert-butoxytris(ethylmethylamido)hafnium and Ozone: Rapid Growth, High Density and Thermal Stability. *J. Mater. Chem.* **2008**, *18*, 4324.
(31) Beladiya, V.; Becker, M.; Faraz, T.; Kessels, W. M. M.; Schenk, P.; Otto, F.; Fritz, T.; Gruenewald, M.; Helbing, C.; Jandt, K. D.; Tünnermann, A.; Sierka, M.; Szeghalmi, A. Effect of an Electric Field during the Deposition of Silicon Dioxide Thin Films by Plasma Enhanced Atomic Layer Deposition: An Experimental and Computational Study. *Nanoscale* **2020**, *12*, 2089−2102.
(32) Beladiya, V.; Faraz, T.; Kessels, W. M. M.; Tünnermann, A.; Szeghalmi, A. In *Controlling Mechanical, Structural, and Optical Properties of $Al_2O_3$ Thin Films Deposited by Plasma-Enhanced Atomic Layer Deposition with Substrate Biasing*, Proceedings of SPIE 10691, Advances in Optical Thin Films VI; International Society for Optics and Photonics, 2018; p 106910E.
(33) Faraz, T.; Verstappen, Y. G. P.; Verheijen, M. A.; Chittock, N. J.; Lopez, J. E.; Heijdra, E.; van Gennip, W. J. H.; Kessels, W. M. M.; Mackus, A. J. M. Precise Ion Energy Control with Tailored Waveform Biasing for Atomic Scale Processing. *J. Appl. Phys.* **2020**, *128*, No. 213301.
(34) Faraz, T.; Arts, K.; Karwal, S.; Knoops, H. C. M.; Kessels, W. M. M. Energetic Ions during Plasma-Enhanced Atomic Layer Deposition and their Role in Tailoring Material Properties. *Plasma Sources Sci. Technol.* **2019**, *28*, No. 024002.
(35) Karwal, S.; Verheijen, M. A.; Arts, K.; Faraz, T.; Kessels, W. M. M.; Creatore, M. Plasma-Assisted ALD of Highly Conductive $HfN_x$: On the Effect of Energetic Ions on Film Microstructure. *Plasma Chem. Plasma Process.* **2020**, *40*, 697−712.
(36) Belahcen, S.; Vallée, C.; Bsiesy, A.; Chaker, A.; Jaffal, M.; Yeghoyan, T.; Bonvalot, M. Control of Ion Energy during Plasma Enhanced Atomic Layer Deposition: A New Strategy for the Modulation of TiN Growth Delay on $SiO_2$. *J. Vac. Sci. Technol., A* **2021**, *39*, No. 012410.
(37) Ratzsch, S.; Kley, E.-B.; Tünnermann, A.; Szeghalmi, A. Inhibition of Crystal Growth during Plasma Enhanced Atomic Layer Deposition by Applying BIAS. *Materials* **2015**, *8*, 7805−7812.
(38) Karwal, S.; Verheijen, M. A.; Williams, B. L.; Faraz, T.; Kessels, W. M. M.; Creatore, M. Low Resistivity HfNx Grown by Plasma-assisted ALD with External Rf Substrate Biasing. *J. Mater. Chem. C* **2018**, *6*, 3917−3926.
(39) Kim, Y.; Kwon, H.; Han, H. S.; Kim, H. J. K.; Kim, B. S. Y.; Lee, B. C.; Lee, J.; Asheghi, M.; Prinz, F. B.; Goodson, K. E.; Lim, J.; Sim, U.; Park, W. Tunable Dielectric and Thermal Properties of Oxide Dielectrics via Substrate Biasing in Plasma-Enhanced Atomic Layer Deposition. *ACS Appl. Mater. Interfaces* **2020**, *12*, 44912−44918.
(40) Legallais, M.; Mehdi, H.; David, S.; Bassani, F.; Labau, S.; Pelissier, B.; Baron, T.; Martinez, E.; Ghibaudo, G.; Salem, B. Improvement of AlN Film Quality Using Plasma Enhanced Atomic Layer Deposition with Substrate Biasing. *ACS Appl. Mater. Interfaces* **2020**, *12*, 39870−39880.
(41) Profijt, H. B.; van de Sanden, M. C. M.; Kessels, W. M. M. Substrate-biasing during Plasma-assisted Atomic Layer Deposition to Tailor Metal-oxide Thin Film Growth. *J. Vac. Sci. Technol., A* **2012**, *31*, No. 01A106.
(42) Chou, C.-Y.; Chang, T.-J.; Wang, C.-I.; Wang, C.-Y.; Yin, Y.-T.; Chung, T.-F.; Yang, J.-R.; Lin, H.-C.; Chen, M.-J. Dielectric Properties and Reliability Enhancement of Atomic Layer Deposited Thin Films by In situ Atomic Layer Substrate Biasing. *J. Mater. Chem. C* **2020**, *8*, 13025−13032.
(43) Pelletier, J. Substrate Biasing during Plasma Processing: Interest, Methods and Limitations. In *Advanced Technologies Based on Wave and Beam Generated Plasmas*; Schlüter, H.; Shivarova, A., Eds.; Nato Science Partnership Subseries: 3; Springer: Netherlands, 2010; Vol *67*, pp 137−148.
(44) Profijt, H. B.; van de Sanden, M. C. M.; Kessels, W. M. M. Substrate Biasing during Plasma-Assisted ALD for Crystalline Phase-Control of TiO2 Thin Films. *Electrochem. Solid-State Lett.* **2011**, *15*, G1−G3.


https://doi.org/10.1021/acsami.1c21889
*ACS Appl. Mater. Interfaces* 2022, 14, 14677−14692

(45) Yeghoyan, T.; Pesce, V.; Jaffal, M.; Lefevre, G.; Gassilloud, R.; Posseme, N.; Bonvalot, M.; Vallée, C. Low temperature Topographically Selective Deposition by Plasma Enhanced Atomic Layer Deposition with Ion Bombardment Assistance. *J. Vac. Sci. Technol., A* **2021**, *39*, No. 032416.
(46) Vallée, C.; Bonvalot, M.; Belahcen, S.; Yeghoyan, T.; Jaffal, M.; Vallat, R.; Chaker, A.; Lefèvre, G.; David, S.; Bsiesy, A.; Possémé, N.; Gassilloud, R.; Granier, A. Plasma Deposition—Impact of Ions in Plasma Enhanced Chemical Vapor Deposition, Plasma Enhanced Atomic Layer Deposition, and Applications to Area Selective Deposition. *J. Vac. Sci. Technol., A* **2020**, *38*, No. 033007.
(47) Schwartzkopf, M.; Wöhnert, S.-J.; Waclawek, V.; Carstens, N.; Rothkirch, A.; Rubeck, J.; Gensch, M.; Drewes, J.; Polonskyi, O.; Strunskus, T.; Hinz, A. M.; Schaper, S. J.; Körstgens, V.; Müller-Buschbaum, P.; Faupel, F.; Roth, S. V. Real-time Insight into Nanostructure Evolution during the Rapid Formation of Ultra-Thin Gold Layers on Polymers. *Nanoscale Horiz.* **2021**, *6*, 132−138.
(48) Schwartzkopf, M.; Santoro, G.; Brett, C. J.; Rothkirch, A.; Polonskyi, O.; Hinz, A.; Metwalli, E.; Yao, Y.; Strunskus, T.; Faupel, F.; Müller-Buschbaum, P.; Roth, S. V. Real-Time Monitoring of Morphology and Optical Properties during Sputter Deposition for Tailoring Metal-Polymer Interfaces. *ACS Appl. Mater. Interfaces* **2015**, *7*, 13547−13556.
(49) Schwartzkopf, M.; Hinz, A.; Polonskyi, O.; Strunskus, T.; Löhrer, F. C.; Körstgens, V.; Müller-Buschbaum, P.; Faupel, F.; Roth, S. V. Role of Sputter Deposition Rate in Tailoring Nanogranular Gold Structures on Polymer Surfaces. *ACS Appl. Mater. Interfaces* **2017**, *9*, 5629−5637.
(50) Schmitt, P.; Stempfhuber, S.; Felde, N.; Szeghalmi, A. V.; Kaiser, N.; Tünnermann, A.; Schwinde, S. Influence of Seed Layers on the Reflectance of Sputtered Aluminum Thin Films. *Opt. Express* **2021**, *29*, 19472−19485.
(51) Dendooven, J.; Ramachandran, R. K.; Solano, E.; Kurttepeli, M.; Geerts, L.; Heremans, G.; Rongé, J.; Minjauw, M. M.; Dobbelaere, T.; Devloo-Casier, K.; Martens, J. A.; Vantomme, A.; Bals, S.; Portale, G.; Coati, A.; Detavernier, C. Independent Tuning of Size and Coverage of Supported Pt Nanoparticles using Atomic Layer Deposition. *Nat. Commun.* **2017**, *8*, No. 1074.
(52) Schmitt, P.; Beladiya, V.; Felde, N.; Paul, P.; Otto, F.; Fritz, T.; Tünnermann, A.; Szeghalmi, A. V. Influence of Substrate Materials on Nucleation and Properties of Iridium Thin Films Grown by ALD. *Coatings* **2021**, *11*, No. 173.
(53) Ristau, D.; Jupé, M.; Starke, K. Laser Damage Thresholds of Optical Coatings. *Thin Solid Films* **2009**, *518*, 1607−1613.
(54) Jena, S.; Tokas, R. B.; Rao, K. D.; Thakur, S.; Sahoo, N. K. Annealing Effects on Microstructure and Laser-induced Damage Threshold of $HfO_2/SiO_2$ Multilayer Mirrors. *Appl. Opt.* **2016**, *55*, 6108−6114.
(55) Guo, K.; Wang, Y.; Chen, R.; Zhu, M.; Yi, K.; He, H.; Shao, J. Effects of Structural Defects on Laser-Induced Damage of 355-nm High-Reflective Coatings Sputtered on Etched Substrates. *Opt. Mater.* **2019**, *89*, 173−177.
(56) Melninkaitis, A.; Maciulevicius, M.; Rakickas, T.; Miksys, D.; Grigonis, R.; Sirutkaitis, V.; Skrebutenas, A.; Buzelis, R.; Drazdys, R.; Abromavicius, G. In *Comparison of Optical Resistance of Ion Assisted Deposition and Standard Electron Beam Deposition Methods for High Reflectance Dielectric Coatings*, Proceedings of SPIE 5963, Advances in Optical Thin Films II; International Society for Optics and Photonics, 2005; p 59631H.
(57) Stolz, C. J.; Negres, R. A. Ten-year Summary of the Boulder Damage Symposium Annual Thin Film Laser Damage Competition. *Opt. Eng.* **2018**, *57*, No. 121910.
(58) Negres, R. A.; Stolz, C. J.; Batavičiūtė, G.; Melninkaitis, A. In *532-nm, Nanosecond Laser Mirror Thin Film Damage Competition*, Proceedings of SPIE 11514, Laser-induced Damage in Optical Materials 2020; International Society for Optics and Photonics, 2020; p 115140L.
(59) Torchio, P.; Gatto, A.; Alvisi, M.; Albrand, G.; Kaiser, N.; Amra, C. High-Reflectivity $HfO_2/SiO_2$ Ultraviolet Mirrors. *Appl. Opt.* **2002**, *41*, 3256−3261.
(60) Bassiri, R.; Clark, C.; Martin, I. W.; Markosyan, A.; Murray, P. G.; Tessmer, J.; Rowan, S.; Fejer, M. M. In *Investigating the Relationship between Material Properties and Laser-Induced Damage Threshold of Dielectric Optical Coatings at 1064 nm*, Proceedings of SPIE 9632, Laser-Induced Damage in Optical Materials; International Society for Optics and Photonics, 2015; p 963204.
(61) Yao, J.; Shao, J.; He, H.; Fan, Z. Effects of Annealing on Laser-induced Damage Threshold of $TiO_2/SiO_2$ High Reflectors. *Appl. Surf. Sci.* **2007**, *253*, 8911−8914.
(62) Shen, J.; Zhang, Q.; Wang, J.; Yang, T.; Deng, Z.; Zhou, B.; Chen, L. Sol-Gel Processing of Zirconia Coating for HR Mirrors with High Laser Damage Threshold. *J. Sol−Gel Sci. Technol.* **2000**, *19*, 271−274.
(63) Guo, Y. J.; Zu, X. T.; Wang, B. Y.; Jiang, X. D.; Yuan, X. D.; Lv, H. B. Preparation of Sol−Gel $ZrO_2-SiO_2$ Highly Reflective Multilayer Films and Laser-induced Damage Threshold Characteristic. *Optik* **2011**, *122*, 1140−1142.
(64) Zhang, D.; Zhu, M.; Li, Y.; Zhang, W.; Cai, X.; Ye, F.; Liang, G.; Zheng, Z.; Fan, P.; Xia, Z. Laser-induced Damage of 355 nm High-Reflective Mirror Caused by Nanoscale Defect. *J. Wuhan Univ. Technol., Mater. Sci. Ed.* **2017**, *32*, 1057−1060.
(65) Grilli, M. L.; Menchini, F.; Piegari, A.; Alderighi, D.; Toci, G.; Vannini, M. $Al_2O_3/SiO_2$ and $HfO_2/SiO_2$ Dichroic Mirrors for UV Solid-State Lasers. *Thin Solid Films* **2009**, *517*, 1731−1735.
(66) Botha, R.; Thöny, S. S.; Grössl, M.; Mourad, S.; Maissen, C.; Venter, J. I.; Südmeyer, T.; Hoffmann, M.; Bulkin, P. V.; Linz-Dittrich, S.; Bischof, D.; Michler, M.; Rinner, S. J.; Ettemeyer, A. In *Comparative Study of the Laser Damage Threshold and Optical Characteristics of $Ta_2O_5$-$SiO_2$ Multilayers Deposited Using Various Methods*, Proceedings of SPIE 9632, Laser-Induced Damage in Optical Materials; International Society for Optics and Photonics, 2015; p 963203.
(67) Zhao, Y.; Wang, Y.; Gong, H.; Shao, J.; Fan, Z. Annealing Effects on Structure and Laser-induced Damage Threshold of $Ta_2O_5/SiO_2$ Dielectric Mirrors. *Appl. Surf. Sci.* **2003**, *210*, 353−358.
(68) Ma, B.; Ding, T.; Jiao, H.; Zhou, G.; Shen, Z.; Cheng, X.; Zhang, J.; Liu, H.; Ji, Y.; He, P.; Wang, Z. In *LIDT of $HfO_2/SiO_2$ HR Films by different Test Modes at 1064 nm and 532 nm*, Proceedings of SPIE 7842, Laser-Induced Damage in Optical Materials; International Society for Optics and Photonics, 2010; p 78420E.
(69) Zhu, M.; Shao, J.; Yi, K.; Li, X.; Yu, Z.; Zhang, W.; Qi, H. In *Research on the Laser Damage Performance of High Reflection Coatings at 355 nm*, Proceedings of SPIE 8786, Pacific Rim Laser Damage 2013: Optical Materials for High Power Lasers; International Society for Optics and Photonics, 2013; p 87860X.
(70) Shestaeva, S.; Bingel, A.; Munzert, P.; Ghazaryan, L.; Patzig, C.; Tünnermann, A.; Szeghalmi, A. Mechanical, Structural, and Optical Properties of PEALD Metallic Oxides for Optical Applications. *Appl. Opt.* **2017**, *56*, C47−C59.
(71) Abadias, G.; Chason, E.; Keckes, J.; Sebastiani, M.; Thompson, G. B.; Barthel, E.; Doll, G. L.; Murray, C. E.; Stoessel, C. H.; Martinu, L. Review Article: Stress in Thin Films and Coatings: Current Status, Challenges, and Prospects. *J. Vac. Sci. Technol., A* **2018**, *36*, No. 020801.
(72) Oliver, J. B.; Kupinski, P.; Rigatti, A. L.; Schmid, A. W.; Lambropoulos, J. C.; Papernov, S.; Kozlov, A.; Smith, C.; Hand, R. D. Stress Compensation in Hafnia/Silica Optical Coatings by Inclusion of Alumina Layers. *Opt. Express* **2012**, *20*, 16596.
(73) Mirkarimi, P. B.; Montcalm, C. In *Advances in the Reduction and Compensation of Film Stress in High-Reflectance Multilayer Coatings for Extreme-Ultraviolet Lithography*, Proceedings of SPIE 3331, Emerging Lithographic Technologies II; International Society for Optics and Photonics, 1998; pp 133−148.
(74) de Denus-Baillargeon, M.; Schmitt, T.; Larouche, S.; Martinu, L. Design and Fabrication of Stress-Compensated Optical Coatings:


https://doi.org/10.1021/acsami.1c21889
ACS Appl. Mater. Interfaces 2022, 14, 14677−14692

Fabry-Perot Filters for Astronomical Applications. *Appl. Opt.* **2014**, *53*, 2616−2624.
(75) Begou, T.; Krol, H.; Stojcevski, D.; Lemarchand, F.; Lequime, M.; Grezes-Besset, C.; Lumeau, J. Complex Optical Interference Filters with Stress Compensation for Space Applications. *CEAS Space J.* **2017**, *9*, 441−449.
(76) Begou, T.; Lemarchand, F.; Lemarquis, F.; Moreau, A.; Lumeau, J. High-Performance Thin-film Optical Filters with Stress Compensation. *J. Opt. Soc. Am. A* **2019**, *36*, C113−C121.
(77) Trubetskov, M.; Amotchkina, T.; Tikhonravov, A.; Veisz, L.; Pervak, V. In *Design, Production, and Reverse Engineering of a Double Sided Innovative Thin Film Laser Element*, Proceedings of SPIE 9627, Optical Systems Design 2015: Advances in Optical Thin Films V; International Society for Optics and Photonics, 2015; p 96270X.
(78) Liu, H.; Jensen, L.; Ma, P.; Ristau, D. Stress Compensated Anti-reflection Coating for High Power Laser Deposited with IBS $SiO_2$ And ALD $Al_2O_3$. *Appl. Surf. Sci.* **2019**, *476*, 521−527.
(79) Cui, H.; Li, B.; Xiao, S.; Han, Y.; Wang, J.; Gao, C.; Wang, Y. Simultaneous Mapping of Reflectance, Transmittance and Optical Loss of Highly Reflective and Anti-Reflective Coatings with Two-Channel Cavity Ring-Down Technique. *Opt. Express* **2017**, *25*, 5807−5820.
(80) Han, Y.; Li, B.; Lifeng, G.; Xiong, S. Reflectivity Mapping of Large-aperture Mirrors with Cavity Ringdown Technique. *Appl. Opt.* **2017**, *56*, C35−C40.
(81) Kim, J.; Kim, S.; Jeon, H.; Cho, M.-H.; Chung, K.-B.; Bae, C. Characteristics of $HfO_2$ Thin Films Grown by Plasma Atomic Layer Deposition. *Appl. Phys. Lett.* **2005**, *87*, No. 053108.
(82) Park, S.; Park, B.-E.; Yoon, H.; Lee, S.; Nam, T.; Cheon, T.; Kim, S.-H.; Cheon, H.; Im, S.; Seong, T.; Kim, H. Comparative Study on Atomic Layer Deposition of $HfO_2$ via Substitution of Ligand Structure with Cyclopentadiene. *J. Mater. Chem. C* **2020**, *8*, 1344−1352.
(83) Naumann, F.; Reck, J.; Gargouri, H.; Gruska, B.; Blümich, A.; Mahmoodinezhad, A.; Janowitz, C.; Henkel, K.; Flege, J. I. In situ Real-time and Ex situ Spectroscopic Analysis of $Al_2O_3$ Films Prepared by Plasma Enhanced Atomic Layer Deposition. *J. Vac. Sci. Technol., B* **2020**, *38*, No. 014014.
(84) Heil, S. B. S.; van Hemmen, J. L.; Hodson, C. J.; Singh, N.; Klootwijk, J. H.; Roozeboom, F.; van de Sanden, M. C. M.; Kessels, W. M. M. Deposition of TiN and $HfO_2$ in a Commercial 200 mm Remote Plasma Atomic Layer Deposition Reactor. *J. Vac. Sci. Technol., A* **2007**, *25*, 1357.
(85) Kim, K.-M.; Jang, J. S.; Yoon, S.-G.; Yun, J.-Y.; Chung, N.-K. Structural, Optical and Electrical Properties of $HfO_2$ Thin Films Deposited at Low-Temperature Using Plasma-Enhanced Atomic Layer Deposition. *Materials* **2020**, *13*, No. 2008.
(86) Martínez, F. L.; Toledano-Luque, M.; Gandía, J. J.; Cárabe, J.; Bohne, W.; Röhrich, J.; Strub, E.; Mártil, I. Optical Properties and Structure of $HfO_2$ Thin Films Grown by High Pressure Reactive Sputtering. *J. Phys. D: Appl. Phys.* **2007**, *40*, 5256.
(87) Jerman, M.; Qiao, Z.; Mergel, D. Refractive Index of Thin Films of $SiO_2$, $ZrO_2$, And $HfO_2$ as a Function of the Films' Mass Density. *Appl. Opt.* **2005**, *44*, 3006−3012.
(88) Stenzel, O.; Wilbrandt, S.; Yulin, S.; Kaiser, N.; Held, M.; Tünnermann, A.; Biskupek, J.; Kaiser, U. Plasma Ion Assisted Deposition of Hafnium Dioxide using Argon and Xenon as Process Gases. *Opt. Mater. Express* **2011**, *1*, 278−292.
(89) Iwashita, S.; Moriya, T.; Kikuchi, T.; Kagaya, M.; Noro, N.; Hasegawa, T.; Uedono, A. Effect of Ion Energies on the Film Properties of Titanium Dioxides Synthesized via Plasma Enhanced Atomic Layer Deposition. *J. Vac. Sci. Technol., A* **2018**, *36*, No. 021515.
(90) Xie, Y.; Ma, Z.; Su, Y.; Liu, Y.; Liu, L.; Zhao, H.; Zhou, J.; Zhang, Z.; Li, J.; Xie, E. The Influence of Mixed Phases on Optical Properties of HfO2 Thin Films Prepared by Thermal Oxidation. *J. Mater. Res.* **2011**, *26*, 50−54.
(91) Balogh-Michels, Z.; Stevanovic, I.; Borzi, A.; Bächli, A.; Schachtler, D.; Gischkat, T.; Neels, A.; Stuck, A.; Botha, R. Crystallization Behavior of Ion Beam Sputtered $HfO_2$ Thin Films and its Effect on the Laser-Induced Damage Threshold. *J. Eur. Opt. Soc.-Rapid Publ.* **2021**, *17*, No. 3.
(92) Zhang, Y.; Weber, W. J. Defect Accumulation, Amorphization and Nanostructure Modification of Ceramics. In *Ion Beam Modification of Solids: Ion−Solid Interaction and Radiation Damage*; Wesch, W.; Wendler, E., Eds.; Springer Series in Surface Sciences; Springer, 2016; Vol. *61*, pp 287−318.
(93) Gago, R.; Jiménez, I.; Albella, J. M. Thin Film Growth by Ion-Beam-Assisted Deposition Techniques. In *Materials Surface Processing by Directed Energy Techniques*; Pauleau, Y., Ed.; EMRS Books Series; Elsevier, 2006; Chapter 10, Vol. *63*, pp 345−382.
(94) Kucheyev, S. Ion-Beam Processing. In *Materials Processing Handbook*; Groza, J. R., Ed.; CRC Press, 2007; pp 3-1−3-16.
(95) Mironov, V. L.; Udalov, O. G.; Gribkov, B. A.; Fraerman, A. A. Comparative X-ray Reflectometry and Atomic Force Microscopy of Surfaces with Non-Gaussian Roughness. *J. Appl. Phys.* **2008**, *104*, No. 064301.
(96) Nie, X.; Ma, F.; Ma, D.; Xu, K. Thermodynamics and Kinetic Behaviors of Thickness-dependent Crystallization in High-k Thin Films Deposited by Atomic Layer Deposition. *J. Vac. Sci. Technol., A* **2015**, *33*, No. 01A140.
(97) Karwal, S.; Karasulu, B.; Knoops, H. C. M.; Vandalon, V.; Kessels, W. M. M.; Creatore, M. Atomic insights into the oxygen incorporation in atomic layer deposited conductive nitrides and its mitigation by energetic ions. *Nanoscale* **2021**, *13*, 10092−10099.
(98) Jena, S.; Tokas, R. B.; Tripathi, S.; Rao, K. D.; Udupa, D. V.; Thakur, S.; Sahoo, N. K. Influence of Oxygen Partial Pressure on Microstructure, Optical Properties, Residual Stress and Laser Induced Damage Threshold of Amorphous $HfO_2$ Thin Films. *J. Alloys Compd.* **2019**, *771*, 373−381.
(99) Iliescu, C.; Avram, M.; Chen, B.; Popescu, A.; Dumitrescu, V.; Poenar, D. P.; Sterian, A.; Vrtacnik, D.; Amon, S.; Sterian, P. Residual Stress In thin Films PECVD Depositions: A Review. *J. Optoelectron. Adv. Mater.* **2011**, *13*, 387−394.
(100) Windischmann, H. Intrinsic Stress in Sputter-deposited Thin Films. *Crit. Rev. Solid State Mater. Sci.* **1992**, *17*, 547−596.
(101) Mbam, S. O.; Nwonu, S. E.; Orelaja, O. A.; Nwigwe, U. S.; Gou, X.-F. Thin-film Coating; Historical Evolution, Conventional Deposition Technologies, Stress-state Micro/nano-level Measurement/models and Prospects Projection: A Critical Review. *Mater. Res. Express* **2019**, *6*, No. 122001.
(102) Koster, M.; Urbassek, H. M. Ion Peening and Stress Relaxation Induced by Low-energy Atom Bombardment of Covalent Solids. *Phys. Rev. B* **2001**, *63*, No. 224111.
(103) Sridhar, G.; Agarwalla, S. K.; Singh, S.; Gantayet, L. M. Cavity Ring-down Technique for Measurement of Reflectivity of High Reflectivity Mirrors with High Accuracy. *Pramana* **2010**, *75*, 1233−1239.
(104) Guenther, K. H. Nodular Defects in Dielectric Multilayers and Thick Single Layers. *Appl. Opt.* **1981**, *20*, 1034−1038.
(105) Stolz, C. J.; Feigenbaum, E. Impact of High Refractive Coating Material on the Nodular-induced Electric Field Enhancement for Near Infrared Multilayer Mirrors. *Appl. Opt.* **2020**, *59*, A20−A25.
(106) Gritsenko, V. A.; Perevalov, T. V.; Islamov, D. R. Electronic Properties of Hafnium Oxide: A Contribution from Defects and Traps. *Phys. Rep.* **2016**, *613*, 1−20.
(107) Takeuchi, H.; Ha, D.; King, T.-J. Observation of Bulk $HfO_2$ Defects by Spectroscopic Ellipsometry. *J. Vac. Sci. Technol., A* **2004**, *22*, 1337−1341.
(108) Bublitz, S.; Mühlig, C. Absolute Absorption Measurements in Optical Coatings by Laser Induced Deflection. *Coatings* **2019**, *9*, No. 473.
(109) Stolz, C. J.; Tench, R. J.; Kozlowski, M. R.; Fornier, A. In *Comparison of Nodular Defect Seed Geometries from Different Deposition Techniques*, Proceedings of SPIE 2714, 27th Annual Boulder Damage Symposium: Laser-Induced Damage in Optical Materials; International Society for Optics and Photonics, 1996; pp 374−382.


https://doi.org/10.1021/acsami.1c21889
*ACS Appl. Mater. Interfaces* 2022, 14, 14677−14692

(110) Cheng, X.; Tuniyazi, A.; Wei, Z.; Zhang, J.; Ding, T.; Jiao, H.; Ma, B.; Li, H.; Li, T.; Wang, Z. Physical Insight toward Electric Field Enhancement at Nodular Defects in Optical Coatings. *Opt. Express* **2015**, *23*, 8609−8619.
(111) Cao, M.; Cao, J.; Liu, M.; Sun, Y.; Wu, M.; Guo, S.; Gao, S. Wavelength Dependence of Nanosecond Laser Induced Surface Damage in Fused Silica from 260 to 1550 nm. *J. Appl. Phys.* **2018**, *123*, No. 135105.
(112) Jensen, L.; Schrameyer, S.; Jupé, M.; Blaschke, H.; Ristau, D. In *Spot-Size Dependence of the LIDT from the NIR to the UV*, Proceedings of SPIE 7504, Laser-Induced Damage in Optical Materials; International Society for Optics and Photonics, 2009; p 75041E.


https://doi.org/10.1021/acsami.1c21889
*ACS Appl. Mater. Interfaces* 2022, 14, 14677−14692